(12)

Report No. NADC-81284-30

Mathematical Foundations for Normal Mode Modelling in Waveguides

Thomas B. Gabrielson

Sensors and Avionics Technology Directorate
Naval Air Development Center
Warminster, Pennsylvania 18974

Phase Report
Airtask No. A03S370A/001B/1WF11-100-000
Work Unit No. ZU21A

Approved for Public Release; Distribution Unlimited

Prepared for
Naval Air Systems Command
Department of the Navy
Washington, D.C. 20361

NOTICES

REPORT NUMBERING SYSTEM – The numbering of technical project reports issued by the Naval Air Development Center is arranged for specific identification purposes. Each number consists of the Center acronym, the calendar year in which the number was assigned, the sequence number of the report within the specific calendar year, and the official 2-digit correspondence code of the Command Office or the Functional Directorate responsible for the report. For example: Report No. NADC-78015-20 indicates the fifteenth Center report for the year 1978, and prepared by the Systems Directorate. The numerical codes are as follows:

CODE	OFFICE OR DIRECTORATE
00	Commander, Naval Air Development Center
01	Technical Director, Naval Air Development Center
02	Comptroller
10	Directorate Command Projects
20	Systems Directorate
30	Sensors & Avionics Technology Directorate
40	Communication & Navigation Technology Directorate
50	Software Computer Directorate
60	Aircraft & Crew Systems Technology Directorate
70	Planning Assessment Resources
80	Engineering Support Group

PRODUCT ENDORSEMENT – The discussion or instructions concerning commercial products herein do not constitute an endorsement by the Government nor do they convey or imply the license or right to use such products.

APPROVED BY: Edward J. Jennings DATE: 2/17/82

REPORT DOCUMENTATION PAGE

READ INSTRUCTIONS BEFORE COMPLETING FORM

1. REPORT NUMBER: NADC-81284-30
2. GOVT ACCESSION NO.:
3. RECIPIENT'S CATALOG NUMBER:

4. TITLE (and Subtitle): MATHEMATICAL FOUNDATIONS FOR NORMAL MODE MODELLING IN WAVEGUIDES
5. TYPE OF REPORT & PERIOD COVERED: Phase
6. PERFORMING ORG. REPORT NUMBER:

7. AUTHOR(s): Thomas B. Gabrielson
8. CONTRACT OR GRANT NUMBER(s):

9. PERFORMING ORGANIZATION NAME AND ADDRESS:
Sensors and Avionics Technology Directorate
Naval Air Development Center
Warminster, Pennsylvania 18974
10. PROGRAM ELEMENT, PROJECT, TASK AREA & WORK UNIT NUMBERS:
AIRTASK NO. A03S370A/001B/
1WF11-100-000 Work Unit No. ZU21A

11. CONTROLLING OFFICE NAME AND ADDRESS:
Naval Air Systems Command
Department of the Navy
Washington, D.C. 20361
12. REPORT DATE:
13. NUMBER OF PAGES:

14. MONITORING AGENCY NAME & ADDRESS (if different from Controlling Office):
15. SECURITY CLASS. (of this report): Unclassified
15a. DECLASSIFICATION/DOWNGRADING SCHEDULE:

16. DISTRIBUTION STATEMENT (of this Report):
Approved for Public Release; Distribution Unlimited

17. DISTRIBUTION STATEMENT (of the abstract entered in Block 20, if different from Report):

18. SUPPLEMENTARY NOTES:
Appendices A,B,C,D,E & F.

19. KEY WORDS (Continue on reverse side if necessary and identify by block number):
NORMAL MODES, ACOUSTIC PROPAGATION MODELS, WAVEGUIDES, INTERFACE WAVES, LATERAL WAVES, LEAKY MODES, STEEPEST DESCENT METHOD

20. ABSTRACT (Continue on reverse side if necessary and identify by block number):
This paper presents the mathematical foundation for wave theory modelling of acoustic propagation in leaky waveguides. In particular, the development of the normal mode solution for the field in a fluid layer overlying a fluid half-space is summarized in order to provide the basis for advanced modelling work. The three types of propagation supported by a leaky duct, trapped modes, leaky modes and interface waves, are developed along with several approximation techniques. Finally, the concepts are illustrated by means of a practical problem in shallow water acoustic transmission.

ABSTRACT

This paper presents the mathematical foundation for wave theory modelling of acoustic propagation in leaky waveguides. In particular, the development of the normal mode solution for the field in a fluid layer overlying a fluid half-space is summarized in order to provide the basis for advanced modelling work. The three types of propagation supported by a leaky duct – trapped modes, leaky modes and interface waves -- are developed along with several approximation techniques. Finally, the concepts are illustrated by means of a practical problem in shallow water acoustic transmission.

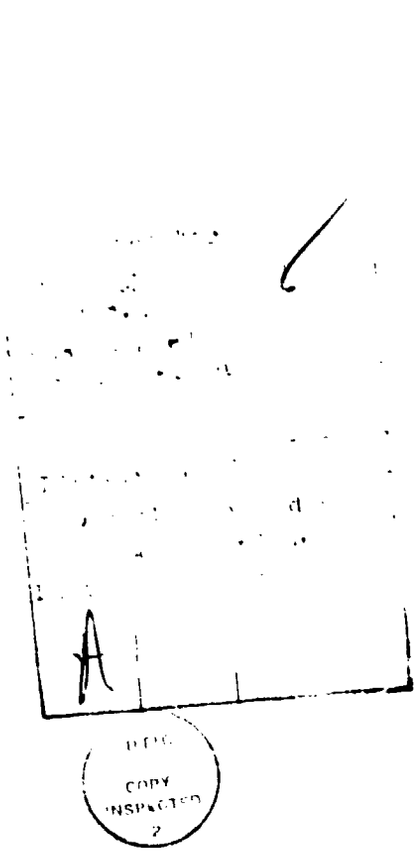

TABLE OF CONTENTS

LIST OF FIGURES

LIST OF SYMBOLS

A	arbitrary function in Hankel and Fourier transform analysis
b	density ratio, ρ_1/ρ_2
BLI	branch line integral
c	sound speed
d	source depth
D	denominator of integrand
D	displacement vector, ui + vj + wk
E	fluid bulk modulus
f	variable exponent in steepest descent method, arbitrary function in transform analysis, frequency
g	arbitrary function in transform analysis
G	function of vertical wave number in fluid layer, factor in integrand of steepest descent integral
H	layer thickness
$H_o^{(1)}$	Hankel function of first kind
$H_o^{(2)}$	Hankel function of second kind
i	$\sqrt{-1}$
J_o	zero order Bessel function of first kind
k	wave number ω/c
K	wave number vector
n	index of eigenvalues
N	numerator of integrand
P	pressure
r	radial distance from z axis
R	slant range
$\vec{R}$	range vector

s	parameter for descent path
t	time
V	reflection coefficient
z	depth
Z	depth function proportional to pressure
α	grazing angle
α_{BP}	critical angle
α_o	saddle point
β	vertical wave number
γ	horizontal wave number
θ	angular position coordinate (cylindrical coordinates)
ν	$i\beta$
ξ	transform function in method of steepest descent
ρ	density
ϕ	angular coordinate for wave number (cylindrical coordinates)
ϕ	time-independent velocity potential
ψ	velocity potential
ω	angular frequency, $2\pi f$

SUMMARY

Following increased activity in underwater acoustics research during World War II, wave theory modeling of acoustic propagation has become an important part of sonar system design and evaluation. Since then, wave propagation analysis of sound in the ocean has been applied to the interpretation of marine geophysical measurements and is now an established tool in underwater oil exploration. This paper presents a survey of the development of wave theory analysis for acoustic propagation in a homogeneous layer of fluid overlying a homogeneous fluid half-space. Although this model of the ocean is highly simplified, the analysis describes the important features of the sound field and forms the basis for constructing more sophisticated models of the ocean environment.

Beginning with the axially symmetric wave equation, the elementary cylindrical wave solution is found by separation of variables. Following the technique developed by Lamb [1], through an integral summation of these elementary wave functions the point harmonic source is replaced by a horizontal boundary plane. In this manner, the solution of a homogeneous differential equation rather than an inhomogeneous equation is required. The resulting solution, a Hankel transform integral, may be evaluated by residue theory in the complex wave number plane.

In general, the form of the solution depends upon the path of the branch cut. Pekeris [2] employed a cut that yields a three part solution in which each part corresponds to a distinct type of propagation. Thus, a finite number of real poles gives rise to a set of modes representing waves trapped in the layer. An infinite number of modes with complex eigenvalues describe energy leakage out of the layer and, finally, a branch line integral contains the contribution of the interface wave. After the Pekeris cut has been examined, the solution resulting from a different branch cut path proposed by Ewing, Jardetsky and Press [3] is developed. This cut, the EJP branch cut, eliminates the complex modes; however, the simplicity of the previous branch line integral is lost.

Detailed investigation of the wave that travels along the interface between the layer and the half-space requires a slight modification of the model. To isolate the effects of this wave, the surface of the fluid layer is raised to infinity. The resulting integral is asymptotically evaluated by the method of steepest descent and the character of the interface wave is discussed. In addition, these same approximation techniques are applied to the Pekeris branch line integral.

Once the solution techniques for the layered half-space have been developed, they are applied to a practical shallow ocean propagation problem. Through this application, the significance of each type of propagation is illustrated.

Following the analysis, a summary of the types of wave propagation in this simple ocean model is presented. The most significant propagation component at long range consists of trapped waves which lose no energy to the half-space below. At short range, two additional types of propagation are evident. One of these field components is the result of travelling waves that leak out of the layer thereby decaying rapidly with increasing range. The other short range component, the interface wave, is strongly excited only when a mode is near cutoff in the layer.

DESCRIPTION OF THE PHYSICAL PROBLEM

In 1948, C.L. Pekeris published[2] the solution to the problem of the propagation of acoustic waves in a fluid layer in contact with a fluid half-space. This study arose as a consequence of a series of measurements performed by Worzel and Ewing[4] employing explosives in shallow ocean water. Ewing noted that the spectrum of the energy arriving at a fixed point distant from the source was dispersed or spread in time. In other words, each frequency component travelled with its own characteristic speed. Using the theoretical work of Gutenberg[5] and Stoneley[6] on the dispersion of Love waves, Pekeris formulated a model of the ocean environment corresponding to those authors' work. Since Love[7] had demonstrated the existence of trapped, dispersive shear waves in an elastic layer over an elastic half-space, Pekeris chose to analyze the equivalent problem for two fluids.

The resultant analysis successfully explained the observed dispersion and, subsequently, this two fluid model became the foundation for most shallow water acoustic modelling. Later improvements in the analysis included allowing the sound speed to vary in the layer, adding more layers and introducing elastic properties in the lower half-space. In spite of these extensions to the theory, the basic solution technique remains unchanged.

In this paper, we shall consider the analysis of the two fluid model in detail. Specifically, the model consists of one homogeneous fluid layer overlying a half-space containing a second homogeneous fluid. As a consequence of the fluid media, shear waves do not exist in this model. However, if elastic substances were substituted for the fluids, the solution for the shear wave field would be conceptually identical to the compressional wave solution. Excitation of the field is by means of a point source of harmonic waves located in the fluid layer. Also, the combination of a point source and parallel, planar boundaries leads naturally to a solution expressed in cylindrical coordinates.

Normally the ocean floor sediment possesses a higher sound speed than the ocean water itself. Therefore, in our analysis, we will assume that the sound speed of the fluid in the half-space is higher than the sound speed in the layer. While there are instances of a lower sound speed in the sediments compared to the sound speed in the overlying water, usually only the upper, highly saturated sediment layers exhibit this behavior. For this reason we will confine our analysis to the problem of a higher sound speed in the half-space. Additionally, the higher sound speed in the underlying half-space permits the existence of trapped waves which dominate the field at long range.

ANALYSIS

Axially Symmetric Wave Equation

In order to describe a point source in a medium with parallel, planar boundaries, the wave equation can be expressed in cylindrical coordinates. Moreover, since the analysis does not contain any azimuthal variation, the axially symmetric form of the wave equation is sufficient, i.e.,

$$\nabla^2\psi = \frac{1}{r}\frac{\partial}{\partial r}\left(r\frac{\partial\psi}{\partial r}\right) + \frac{\partial^2\psi}{\partial z^2} = \frac{1}{c^2}\frac{\partial^2\psi}{\partial t^2} \tag{1}$$

where

- c = sound speed
- r = radial distance from z axis
- t = time
- z = depth
- ψ = velocity potential.

Use of velocity potential reduces the equation of motion to a scalar rather than a vector equation.

The particle velocity is related to the velocity potential by,

$$-\nabla\psi = \frac{\partial}{\partial t}D = i\frac{\partial u}{\partial t} + j\frac{\partial v}{\partial t} + k\frac{\partial w}{\partial t} \tag{2}$$

where

- D = displacement vector
- u = x component of displacement
- v = y component of displacement
- w = z component of displacement.

Furthermore, the volume expansion or dilatation of a small element of fluid is given by the divergence of the displacement and is related to the pressure in the fluid by,

$$p = -E\nabla \cdot D \tag{3}$$

where

- P = pressure
- E = bulk modulus of fluid.

Also, the sound speed in the fluid is given by,

$$c^2 = \frac{E}{\rho} \tag{4}$$

where

- ρ = density.

Taking the divergence of equation (2), we obtain,

$$\nabla^2\psi = -\frac{\partial}{\partial t} \quad (\nabla \cdot D)$$

Using equation (3) for the pressure and equation (4) for the sound speed in this last result, we find,

$$\nabla^2\psi = \frac{\partial}{\partial t} \left(\frac{p}{\rho c^2}\right)$$

However, equation (1) and this result imply,

$$p = \rho \frac{\partial \psi}{\partial t} \tag{5}$$

Since the point source has been assumed to be harmonic, the time dependence of the potential function can be written as follows,

$$\psi = e^{i\omega t} \Phi (r, z) \tag{6}$$

where

$i = \sqrt{-1}$

ω, angular frequency = $2\pi f$

Φ = harmonic potential.

Introducing this last assumption into the wave equation, i.e., equation (1), we have,

$$\frac{1}{r} \frac{\partial}{\partial r} \left(r \frac{\partial \Phi}{\partial r}\right) + \frac{\partial^2 \Phi}{\partial Z^2} + \frac{\omega^2}{c^2} \Phi = 0 \tag{7}$$

The assumed time variation of equation (6) also leads to a simpler relationship between the acoustic pressure and the potential function than indicated by equation (5):

$$p = i\omega\rho \Phi \tag{8}$$

Applying separation of variables to the time independent differential equation (7) we may write a range equation,

$$r^2 \frac{d^2R}{dr^2} + r \frac{dR}{dr} + \gamma^2 r^2 R = 0$$

and a depth equation,

$$\frac{d^2Z}{dZ^2} + \left(\frac{\omega^2}{c^2} - \gamma^2\right) Z = 0 \tag{9}$$

where

$R(r)$ = function of the radius, r

$Z(z)$ = function of depth, z

γ = horizontal wave number

The range equation is a form of Bessel's equation and the solution, bounded as the range increases to infinity, is given by,

$$R = J_o(\gamma r) \tag{10}$$

where $J_o(\rho)$ = zero order Bessel function of the first kind. On the other hand, both solutions of the depth equation (9) must be retained until we consider the fluid layer problem. These solutions are of the form,

$$Z = e^{\pm i\beta z} \tag{11}$$

where

$$\beta, \text{ vertical wave number} = \sqrt{\frac{\omega^2}{c^2} - \gamma^2} \tag{12}$$

Therefore, an elementary solution to the axial symmetric wave equation can be written by substituting the product of equations (10) and (11) for the harmonic potential, Φ, in equation (6). The result of this operation is,

$$\psi = e^{i\omega t} J_o(\gamma r)\, e^{\pm i\beta z} \tag{13}$$

Observe that the vertical wave number, β, is defined in equation (12) by a square root and, therefore, can be either positive or negative. In order to select the proper sign, we consider only the exponential factors of equation (13) which can be combined as follows,

$$\frac{\psi}{J_o(\gamma r)} = e^{i(\omega t \pm \beta z)} \tag{14}$$

If the wave number, β, is real, the negative sign indicates a wave travelling in the positive z direction while the positive sign refers to a wave travelling in the negative z direction. In some regions of the medium, waves travelling in both directions are physically reasonable; however, in a region beyond any reflectors, there is nothing to cause the wave to return toward the source. For this case, the sign of the wave number must be selected to guarantee waves which travel away from the source. In the event that ω^2/c^2 is less than γ^2, equation (12) produces an imaginary value for β and the depth function, Z, is exponential in behavior. Thus, the sign of the exponent of equation (14) must be chosen to insure a physically reasonable decrease in the amplitude as we depart from the source. This consideration will be discussed in greater detail in connection with the improper or leaky modes of vibration.

The technique we shall employ to develop the solution to the layered problem is generally attributed to Lamb[1]. A point source generates a spherical wave, at least before any boundary interaction occurs, while a cylindrical coordinate system is convenient for the description of the boundary conditions. Therefore, we shall expand a spherical wave in terms of the elementary cylindrical wave functions given by equation (13). This may be accomplished by the application of the Hankel transform according to the procedure outlined in Appendix A. The result of this development, equation (A-12), is

$$\psi = e^{i\omega t} \int_0^\infty \frac{J_o(\gamma r)\, e^{\pm i\beta z}}{i\beta}\, \gamma\, d\gamma \tag{15}$$

Initially, we shall consider the source to be located in the plane, z = 0. Following Pekeris' technique[8], we represent the source as a set of boundary conditions rather than as an inhomogeneous source term in the original differential equation. Thus, we require continuity of the pressure and a discontinuity in the particle velocity across the plane, z = 0, such that the depth function assumes the form,

$$Z = \frac{\gamma}{i\beta} e^{\pm i\beta z}$$

This representation of the depth function guarantees that the z dependence of the resulting potential function is identical to the integral indicated in equation (15). Therefore, the general form for the depth equation is,

$$Z_+ = C_1 e^{-i\beta z} \quad (z > 0)$$

$$Z_- = C_2 e^{i\beta z} \quad (z < 0)$$

Note that the signs in the exponents have been selected to insure that the resulting waves diverge from the source. Continuity of pressure along the plane, z = 0, yields,

$$C_1 = C_2 = \frac{\gamma}{i\beta} \tag{16}$$

Further, the discontinuity in the vertical component of particle velocity can be expressed, using equation (2), in the form,

$$\left.\frac{dZ_-}{dz}\right|_0 - \left.\frac{dZ_+}{dz}\right|_0 = 2\gamma \tag{17}$$

Therefore, we shall introduce a point source into our analysis by placing a horizontal boundary plane through the source and requiring that the two conditions expressed by equations (16) and (17) be satisfied on this source plane.

Formulation of the Boundary Value Problem

Since we have replaced the point source by a boundary surface, we can formulate the problem of a fluid layer overlying a fluid half-space[2]. We shall assume that the fluid layer is bounded above (see figure 1) by air and below by a second fluid with a higher sound speed than the layer. Since the density of air is so much lower than that of water, the fluid in the layer, we shall assume that the pressure on the upper surface of the layer, i.e., the plane, z = 0, is equal to zero. Because the sound speed in the layer is not equal to the sound speed in the underlying half-space, the vertical wave number, β, will have a different value in each region. The expressions for the wave numbers can be written from equation (12) as,

$$\beta_1 = \sqrt{\frac{\omega^2}{c_1^2} - \gamma^2}$$

$$\beta_2 = \sqrt{\frac{\omega^2}{c_2^2} - \gamma^2} \tag{18}$$

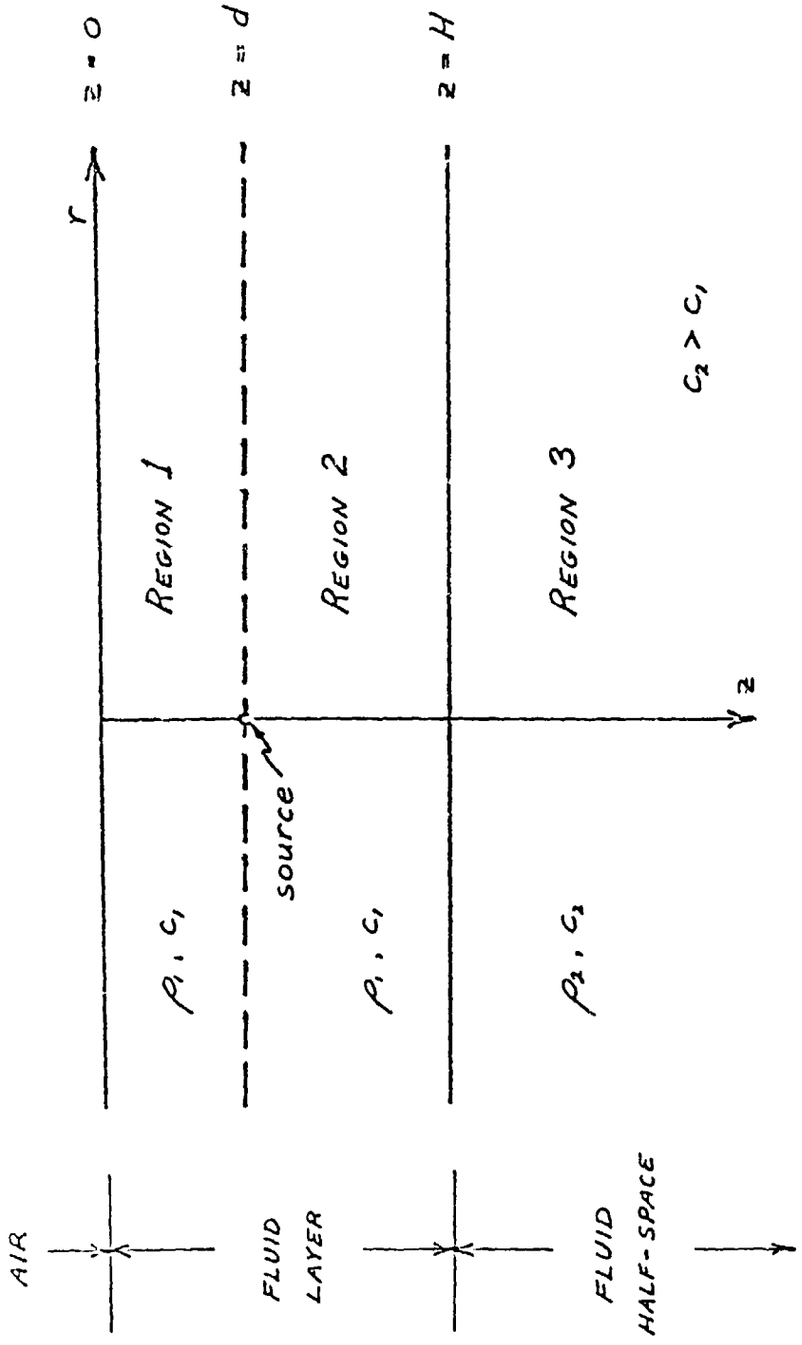

FIGURE 1. — Geometry of the layered half-space

where

c_1 = sound speed in the layer

c_2 = sound speed in the half-space.

In addition, the depth functions, equation (11), may be expressed in the form,

$$\begin{aligned} &\text{Region I} : Z_1 = C_1 \sin\beta_1 z + C_2 \cos\beta_1 z \\ &\text{Region II} : Z_2 = C_3 \sin\beta_1 z + C_4 \cos\beta_1 z \\ &\text{Region III}: Z_3 = C_5 e^{-i\beta_2 z} + C_6 e^{i\beta_2 z} \end{aligned} \tag{19}$$

where the regions are defined in figure 1.

Recalling the previous discussion concerning the sign of the exponent in equation (14), we observe that the second term in the expression for Z_3 represents waves converging on the source from the half-space. Nothing in the half-space can produce waves travelling toward the source, therefore, this second term is meaningless, or

$$C_6 = 0 \tag{20}$$

However, if γ^2 is greater than ω^2/c_2^2, then, by equation (18), β_2 is imaginary and must be written as,

$$\beta_2 = -i\sqrt{\gamma^2 - \frac{\omega^2}{c_2^2}} \tag{21}$$

Notice that the negative square root has been selected in order that when this last result is substituted into the third depth function expression, equation (19), the first term amplitude decreases exponentially with increasing depth in the half-space.

In view of the previous remarks concerning the air-water interface and the representation of the source as a boundary, we may express the conditions along the horizontal boundaries of the three regions as follows:

1) at z = 0 the pressure is equal to zero, or,

$$Z_1(0) = 0 ; \tag{22}$$

2) at the source depth, z = d, in accordance with equations (16) and (17), we have,

$$Z_1(d) = Z_2(d)$$

for continuity of pressure, and,

$$\frac{dZ_1(d)}{dz} - \frac{dZ_2(d)}{dz} = 2\gamma$$

for the discontinuity in particle velocity; and,

3) at the interface, Z = H, separating the layer from the half-space, we express the pressure by means of equation (8),

$$\rho_1 Z_2 (H) = \rho_2 Z_3 (H)$$

for continuity of pressure, and,

$$\frac{dZ_2 (H)}{dz} = \frac{dZ_3(H)}{dz}$$

for continuity of particle velocity.

Introducing the depth functions given by equations (19) into the above boundary conditions, we obtain four equations in four unknowns. Since the first condition, equation (22), leads immediately to $C_2 = 0$, we may write,

$$C_1 \sin \beta_1 d - C_3 \sin \beta_1 d - C_4 \cos \beta_1 d = 0$$

$$\beta_1 C_1 \cos \beta_1 d - \beta_1 C_3 \cos \beta_1 d + \beta_1 C_4 \sin \beta_1 d = 2\gamma$$

$$\rho_1 C_3 \sin \beta_1 H + \rho_1 C_4 \cos \beta_1 H - \rho_2 C_5 e^{-i\beta_2 H} = 0$$

$$\beta_1 C_3 \cos \beta_1 H - \beta_1 C_4 \sin \beta_1 h + i\beta_2 C_5 e^{-i\beta_2 H} = 0$$

The constants are evaluated by solving this system of equations simultaneously. Thus,

$$C_1 = \frac{2\gamma}{\beta_1} \left[\frac{\beta_1 \cos [\beta_1 (H-d)] + ib\beta_2 \sin [\beta_1 (H-d)]}{\beta_1 \cos \beta_1 H + ib\beta_2 \sin \beta_1 H} \right]$$

$$C_3 = \frac{2\gamma \sin \beta_1 d}{\beta_1} \left[\frac{\beta_1 \sin \beta_1 H - ib\beta_2 \cos \beta_1 H}{\beta_1 \cos \beta_1 H + ib\beta_2 \sin \beta_1 H} \right]$$

$$C_4 = \frac{2\gamma \sin \beta_1 d}{\beta_1}$$

$$C_5 = \frac{2\gamma b e^{i\beta_2 H} \sin \beta_1 d}{\beta_1 \cos \beta_1 H + ib\beta_2 \sin \beta_1 H}$$

where

$$b = \rho_1/\rho_2$$

By substituting the values of the above constants in equations (19) and constructing potential functions in the form of equation (13), the velocity potential for each region can be written as,

$$\phi_1 = 2e^{i\omega t} \int_0^\infty J_0 (\gamma r)\, \gamma \frac{\sin \beta_1 z}{\beta_1} \left[\frac{\beta_1 \cos [\beta_1 (H-d)] + ib\beta_2 \sin [\beta_1 (H-d)]}{\beta_1 \cos \beta_1 H + ib\beta_2 \sin \beta_1 H} \right] d\gamma$$

$$(0 < z < d) \qquad (23)$$

$$\psi_2 = 2e^{i\omega t} \int_0^\infty J_c(\gamma r)\gamma \frac{\sin \beta_1 d}{\beta_1} \left[\frac{\beta_1 \cos [\beta_1(H-z)] + ib\beta_2 \sin [\beta_1(H-z)]}{\beta_1 \cos \beta_1 H + ib\beta_2 \sin \beta_1 H} \right] d\gamma$$

$(d < z < H)$ (24)

$$\psi_3 = 2e^{i\omega t} \int_0^\infty J_o(\gamma r)\gamma \left[\frac{b \sin \beta_1 d e^{-i\beta_2(z-H)}}{\beta_1 \cos \beta_1 H + ib\beta_2 \sin \beta_1 H} \right] d\gamma$$

$(H < z)$ (25)

To complete the analysis, we must evaluate the above integrals and, for this purpose, we will transform them into complex contour integrals. We observe, however, that the expression for ψ_2 is identical to the expression for ψ_1 if z and d are interchanged. Thus, in order to compute the field anywhere in the fluid layer, we need only evaluate equation (23) or equation (24). These integrals can be evaluated numerically when r is small and the wavelength is comparable to the layer depth, H. In all other cases, the integrand oscillates rapidly and is difficult to integrate numerically.

Integration in the Complex Wave Number Plane

Before integrating equations (23), (24), and (25), it is useful to replace the Bessel function, J_o, by Hankel functions[9]. The Hankel functions are related to the Bessel function as follows,

$$J_o(\gamma r) = \frac{1}{2} \left[H_o^{(1)}(\gamma r) + H_o^{(2)}(\gamma r) \right] \quad (26)$$

$$H_o^{(1)}(\gamma r) = -H_o^{(2)}(-\gamma r) \quad (27)$$

where

$H_o^{(1)}$ = Hankel function of the first kind

$H_o^{(2)}$ = Hankel function of the second kind

For large values of the argument, γr, the Hankel functions may be replaced by asymptotic approximations of the form,

$$H_o^{(1)}(\gamma r) \simeq \sqrt{\frac{2}{\pi \gamma r}} e^{i\left(\gamma r - \frac{\pi}{4}\right)} \quad (28)$$

$$H_o^{(2)}(\gamma r) \simeq \sqrt{\frac{2}{\pi \gamma r}} e^{-i\left(\gamma r - \frac{\pi}{4}\right)} \quad (29)$$

where

$\gamma r >> 1$

First, let us rewrite equation (24) through the use of equation (26),

$$\psi_2 = e^{i\omega t}\left\{ \int_0^\infty H_0^{(1)}(\gamma r)\gamma\, G(\beta_1, \beta_2)\, d\gamma + \int_0^\infty H_0^{(2)}(\gamma r)\gamma\, G(\beta_1, \beta_2)\, d\gamma \right\} \quad (d < z < H)$$

where

$$G(\beta_1, \beta_2) = \frac{\sin \beta_1 d}{\beta_1} \left[\frac{\beta_1 \cos [\beta_1(H-z)] + ib\beta_2 \sin [\beta_1(H-z)]}{\beta_1 \cos \beta_1 H + ib\beta_2 \sin \beta_1 H} \right] \tag{30}$$

Relation (27) can be employed to rewrite this integral as follows,

$$\psi_2 = e^{i\omega t} \int_{-\infty}^\infty H_0^{(2)}(\gamma r)\gamma\, G(\beta_1, \beta_2)\, d\gamma \tag{31}$$

In order to establish the behavior of the integrand in the γ-plane, we recall that the definitions of β_1 and β_2 from equations (18) lead to the branch points given below,

$$\gamma_1 = \frac{\omega}{c_1}$$
$$\gamma_2 = \frac{\omega}{c_2} \tag{32}$$

Further, the poles of the integrand are located at the zeros of the denominator of equation (30), or,

$$\beta_1 \cos \beta_1 H + ib\beta_2 \sin \beta_1 H = 0 \tag{33}$$

We will show that the pole at $\beta_1 = 0$ lies outside the contour used to evaluate equation (31), thus, it contributes nothing to the solution.

Pekeris[2] proposed the contour illustrated in figure 2, in which the branch cuts extend downward from the branch points. Observe that as the radius of the circular arc contours, C_1 through C_4, becomes infinite, the path, A, becomes the integration path for the desired potential integral, equation (31). We express this relationship as follows,

$$\Phi_2 = \frac{\psi_2}{e^{i\omega t}} = \int_A = \int_{C_{1234}} + \int_{B_1} + \int_{B_2} - 2\pi i \sum^n (\text{residues})_n$$

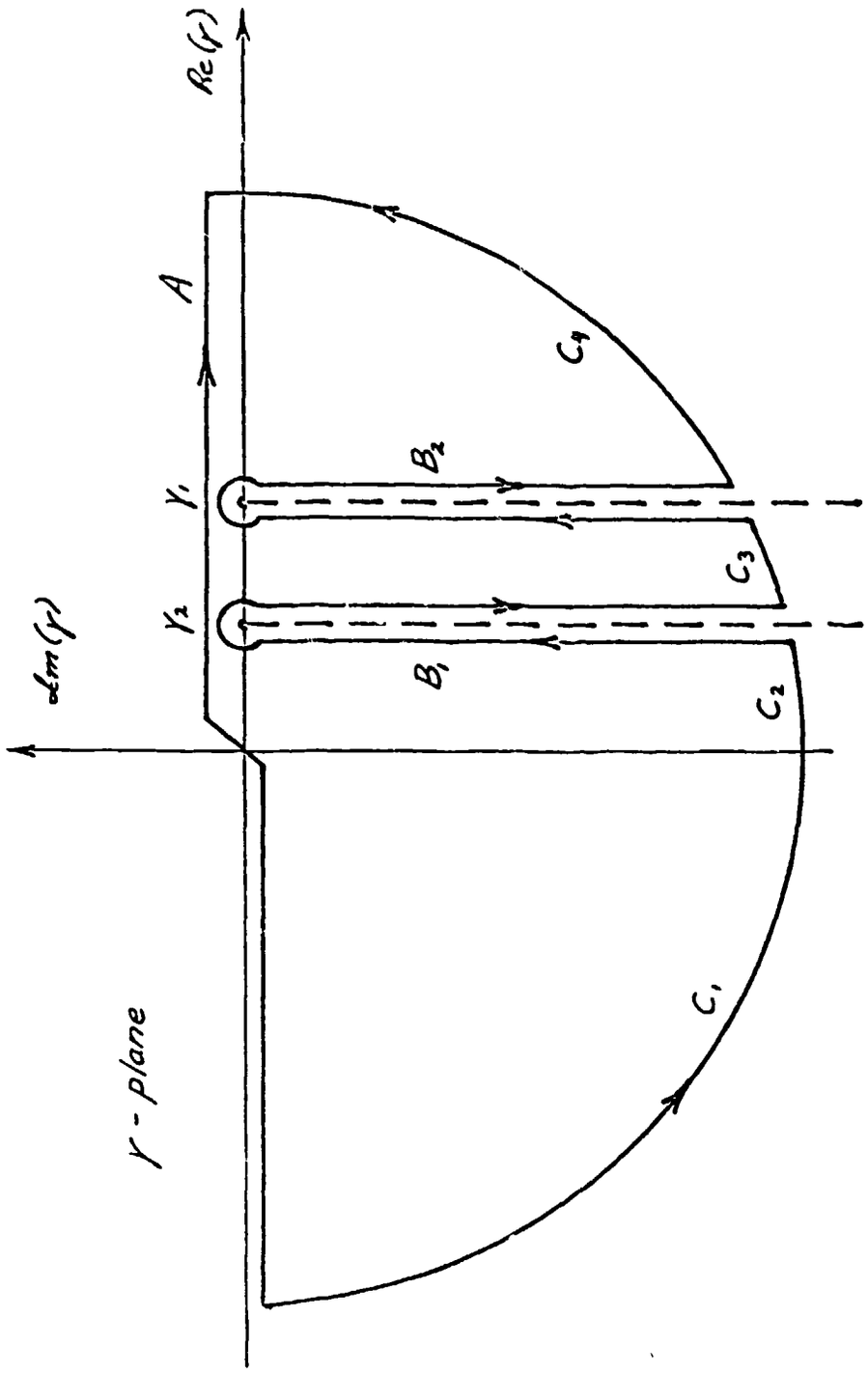

FIGURE 2. – Countour integration in γ-plane: Pekeris Cut

In the above expression the sum includes the residues of all the poles enclosed by the contour. Since the Hankel function decays exponentially for large magnitudes of γ in the third and fourth quadrants as described by equation (29), the integrals over the paths C_1, C_2, C_3 and C_4 approach zero for large radius. (A formal proof for this behavior is presented in Appendix B.) Also, from equation (30), we notice that $G(\beta_1, \beta_2)$ is an even function of β_1, hence, the integral along one side of the branch cut cancels that along the other side. Thus, the solution reduces to,

$$\Phi_2 = -2\pi i \, \Sigma \text{ residues} + \int_{B_1} \tag{34}$$

The residues of equation (31) can be found by rewriting the integrand as,

$$\frac{N(\gamma)}{D(\gamma)}$$

where

$D(\gamma)$ = denominator of equation (30) without the β_1 factor

$N(\gamma)$ = remainder of the integrand.

Therefore,

$$2\pi i(\text{residue})_n = 2\pi i \left. \frac{(\gamma-\gamma_n)\, N(\gamma)}{D(\gamma)} \right|_{\gamma=\gamma_n}$$

$$= 2\pi i \left. \left[\frac{N(\gamma) + (\gamma-\gamma_n) \frac{\partial}{\partial\gamma} N(\gamma)}{\frac{\partial}{\partial\gamma} D(\gamma)} \right] \right|_{\gamma=\gamma_n}$$

$$= 2\pi i \left. \frac{N(\gamma_n)}{\frac{\partial}{\partial\gamma} D(\gamma)} \right|_{\gamma=\gamma_n}$$

By performing the indicated operations, we find,

$$(\text{residue})_n = H_o^{(2)}(\gamma_n r) \, \frac{\beta_1 \sin \beta_1 d \sin \beta_1 z}{H\beta_1 - \cos \beta_1 H \sin \beta_1 H - b^2 \sin^2 \beta_1 H \tan \beta_1 H} \tag{35}$$

where

β_1 is evaluated for $\gamma = \gamma_n$

γ_n is the value of γ at the n^{th} pole.

Furthermore, we observe that β_2 has been eliminated from this equation by using equation (33).

By replacing the Hankel function in equation (35) by its asymptotic form, equation (29), the physical significance of each residue or normal mode can be determined. The range and time dependent factors of each mode may be combined so that the mode is asymptotically proportional to the following expression,

$$(\text{residue})_n \propto \frac{1}{\sqrt{r}} e^{i(\omega t - \gamma_n r)} = \frac{1}{\sqrt{r}} e^{i\omega\left(t - \frac{r}{c_n}\right)} \tag{36}$$

where

$$\gamma_n = \frac{\omega}{c_n} \tag{37}$$

Hence, each mode represents a travelling cylindrical wave with a phase velocity, c_n. In the event that γ_n is real, the wave suffers no attenuation, only the cylindrical spreading given by the $r^{-\frac{1}{2}}$ factor. In other words, the wave is completely trapped in the fluid layer. On the other hand, if γ_n is complex, the wave will be damped because of the appearance of a real exponential factor in equation (36). We observe that the contour in figure 2 was chosen so that the imaginary part of γ will always be negative, thus insuring that a real exponential factor in equation (36), if it exists, decays with increasing range. This explains the selection of $H_0^{(2)}$ in equation (31) since this function passes to zero with large negative, imaginary argument.

Proper evaluation of the branch line integral, depends on the choice of the sign of β_2 on each side of the branch cut. Expressing the horizontal wave number, γ, as a complex number,

$$\gamma = \gamma_r + i\,\gamma_i$$

where

γ_r = real part of γ

γ_i = imaginary part of γ,

we may represent β_2 by employing equation (18),

$$\beta_2^2 = \frac{\omega^2}{c_2^2} - \gamma_r^2 + \gamma_i^2 - 2i\,\gamma_r\,\gamma_i \tag{38}$$

Along the branch cut, $\gamma_r = \omega/c_2$, and γ_i ranges from 0 to $-\infty$, therefore,

$$\beta_2^2 = \gamma_i^2 - 2i\gamma_i \frac{\omega}{c_2} \qquad (-\infty < \gamma_i < 0)$$

This parabola is shown as contour B, in figure 3 and A_+ and A_- represent the two roots of β_2^2, i.e.,

$$A_+ = + \sqrt{\beta_2^2}$$

$$A_- = - \sqrt{\beta_2^2}$$

As demonstrated in Appendix C, the real eigenvalues, γ_n, corresponding to trapped modes are all located on the real axis of the γ-plane to the right of ω/c_2. Substituting $\gamma_i = 0$ and $\gamma_r > \omega/c_2$ into equation (38), we find that this portion of the real axis in the γ-plane transforms to either the positive or negative imaginary axis of the β_2-plane since,

$$\beta_2^2 = \frac{\omega^2}{c_2^2} - \gamma_r^2 < 0 \tag{39}$$

If we recall the depth function in the half-space below the layer, i.e., equations (19) and (20),

$$Z_3 = C_5 e^{-i\beta_2 z} \tag{40}$$

we conclude that, if β_2 is imaginary, it must be negative in order to guarantee the physically reasonable exponential decay with increasing depth in the half-space. Therefore, we select the region below contours A_- and A_+ in figure 3 as the branch for β_2. By substituting the appropriate values for γ_r and γ_i into equation (38), we can show that the path in the γ-plane, labelled number 2 in figure 3, transforms to the positive real axis of the β_2 plane. The transformation between the γ-plane and the β_2-plane is illustrated in figure 3.

On the basis of figure 3, we can summarize the behavior of β_2 in the γ-plane as follows:

Region I: $\beta_{2r} > 0$, $\beta_{2i} > 0$ (use positive root for β_2) (41)

Region II: $\beta_{2r} < 0$, $\beta_{2i} < 0$ (use negative root for β_2) (42)

Region III: $\beta_{2r} > 0$, $\beta_{2i} < 0$ (43)

where

β_{2r} = real part of β_2

β_{2i} = imaginary part of β_2

Now that we have determined which value of β_2 to select on each side of the branch cut, the branch line integral can be specified. As shown in figure 2, the path passes up along the left side of the cut and down along the right, so that the integral in equation (34) becomes,

$$\int_{B_1} = \int_{\frac{\omega}{c_2} - i\infty}^{\frac{\omega}{c_2}} H_o^{(2)}(\gamma r)\, \gamma\, G(\beta_1, \beta_2)\, d\gamma + \int_{\frac{\omega}{c_2}}^{\frac{\omega}{c_2} - i\infty} H_o^{(2)}(\gamma r)\, \gamma\, G(\beta_1, -\beta_2)\, d\gamma$$

$$= \int_{\frac{\omega}{c_2} - i\infty}^{\frac{\omega}{c_2}} H_o^{(2)}(\gamma r)\, \gamma \left[G(\beta_1, \beta_2) - G(\beta_1, -\beta_2) \right] d\gamma$$

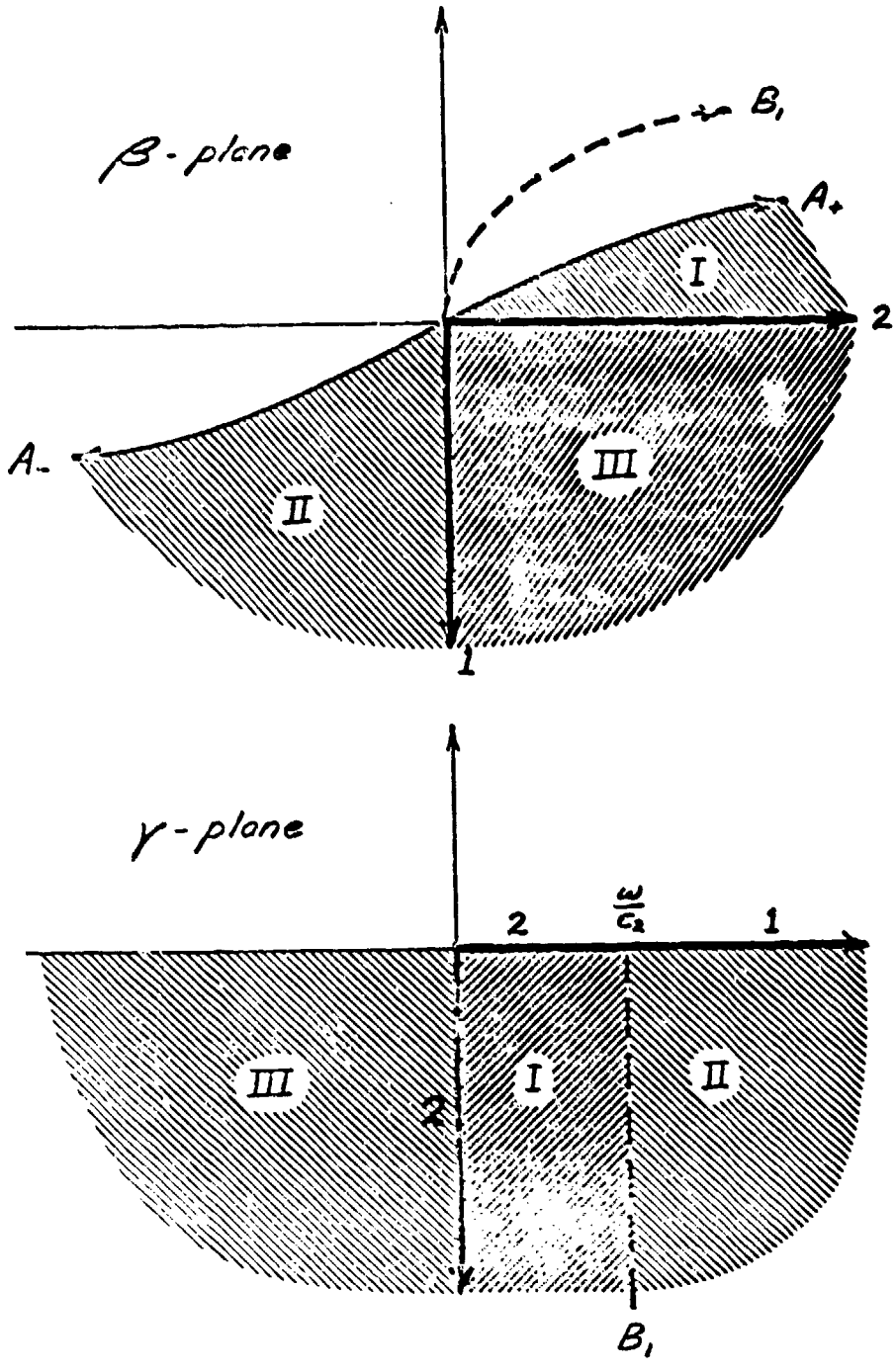

FIGURE 3. – Correspondence between γ and β-planes for the Pekeris cut. B_1 is represented as β^2 in the β-plane and A_+ and A_- represent the two roots of this quantity

By substituting the expression for G (β_1, β_2), equation (30), into this last result and simplifying, the branch line integral can be written as,

$$\int_{B_1} = -2ib \int_{\frac{\omega}{c_2} - i\infty}^{\frac{\omega}{c_2}} H_o^{(2)}(\gamma r)\,\gamma \left[\frac{\beta_2 \sin\beta_1 d \sin\beta_1 z}{\beta_1^2 \cos^2\beta_1 H + b^2\beta_2^2 \sin^2\beta_1 H}\right] d\gamma \qquad (44)$$

Therefore, the complete solution, equation (34), is the combination of this branch line integral and the sum of modes given individually by equation (35). Hence,

$$\Phi(r,z) = -2\pi i \sum^{n} H_o^{(2)}(\gamma_n r) \frac{\beta_1 \sin\beta_1 d \sin\beta_1 z}{H\beta_1 - \cos\beta_1 H \sin\beta_1 H - b^2 \sin\beta_1 H \tan\beta_1 H}$$

$$-2ib \int_{\frac{\omega}{c_2} - i\infty}^{\frac{\omega}{c_2}} H_o^{(2)}(\gamma r)\,\gamma \left[\frac{\beta_2 \sin\beta_1 d \sin\beta_1 z}{\beta_1^2 \cos^2\beta_1 H + b^2\beta_2^2 \sin^2\beta_1 H}\right] d\gamma \qquad (45)$$

According to Appendix C, the roots of the characteristic equation, equation (33), either lie along the real axis between ω/c_2 and ω/c_1 or in region I of the γ-plane shown in figure 3. The former set of solutions is a finite set and represents waves with energy trapped in the layer while the latter set of solutions is infinite. Each mode of this infinite set spreads cylindrically, i.e., its amplitude varies as $r^{-\frac{1}{2}}$, as do the trapped modes. However, these modes, which are not trapped, also decay exponentially with increasing range because the eigenvalue, γ_n, has a negative imaginary part. These modes corresponding to complex eigenvalues are called "leaky" or "improper" modes. Such modes are leaky because the energy is not completely trapped in the layer and improper because of their behavior as depth in the half-space increases.

Consider the vertical wave number, β_2, in region I of the γ-plane, the region in which these improper modes are found. In this region, both the real and imaginary parts of β_2 are positive as expressed by equation (41). Hence, the depth function in the half-space, i.e., equation (40), in combination with the time dependence is of the form,

$$Z_3 = e^{i\omega t} e^{-i\beta_2 z} = e^{i(\omega t - \beta_{2r} z)} e^{\beta_{2i} z}$$

This last expression describes a wave diverging from the source as it should; however, the last factor indicates that it increases exponentially with depth. Such unphysical behavior for a mode leads to its being termed an improper mode. It has been found that the sum of these improper modes is well behaved at large depths. Indeed, useful results have been obtained for the field in the layer by adding these modes and the trapped modes[10, 11].

As we have observed, the improper modes are found to lie in region I of the γ-plane and examination of figure 3 suggests that this region could be eliminated by re-routing the branch cut. If the cut is taken from ω/c_2 along the real axis to the origin and then down the negative imaginary axis to infinity, the contour, A_+, in the β_2-plane would lie along the positive real axis and A_- would coincide with the negative real axis. As a result, region I disappears and the only modes remaining correspond to trapped modes with poles on the real axis.

This cut was proposed by Ewing, Jardetzky and Press[3] and is called the EJP cut in this paper while the cut considered previously is called the Pekeris cut. The branch line integral is identical in form to the Pekeris branch line integral, equation (44); however, the limits of integration are modified to follow the EJP cut. Thus, the EJP branch line integral is given by,

$$\int_{EJP} = -2ib \int_{-i\infty}^{\frac{\omega}{c_2}} H_0^{(2)}(\gamma r)\,\gamma \left[\frac{\beta_2 \sin \beta_1 d \sin \beta_1 z}{\beta_1^2 \cos^2 \beta_1 H + b^2 \beta_2^2 \sin^2 \beta_1 H}\right] d\gamma \qquad (46)$$

The EJP cut is shown as path 2 in figure 3. Although the prospect of not having to locate and evaluate complex eigenvalues is attractive, the branch line integral for the EJP cut is much more difficult to evaluate numerically than the Pekeris branch line integral, particularly at high frequencies[12]. This is true because the Hankel function oscillates much more rapidly when the real part of its argument is varied, as in the final segment of the EJP cut along the real axis, than when the imaginary part is changed.

Reflection of a Spherical Wave

We have completed the solution to the problem of a layer overlying a half-space, but we have not interpreted the branch line integral, equation (44), physically. In order to gain some insight into the interaction of waves with the interface, it is necessary to simplify the problem somewhat. To accomplish this purpose, we shall let the layer thickness become infinite. In this case, the problem reduces to one of two half-spaces and, as a result, the complications of waves returning from surface reflections are avoided.

Another benefit of this simplification is that the lower half-space need no longer be homogeneous provided that it can be characterized by a plane wave reflection coefficient. We gain this generalization by expanding the spherical wave from a point source in terms of plane waves rather than in terms of cylindrical waves. From the derivation in Appendix D, a spherical wave can be expressed as equation (D-6) which is repeated below,

$$\frac{e^{-ikR}}{R} = \frac{1}{2\pi} \iint_{-\infty}^{\infty} \frac{e^{-iK \cdot \delta R}}{i\beta}\, d\gamma_x\, d\gamma_y \qquad (47)$$

where

K, vector wave number = $\gamma_x i + \gamma_y j + \beta k$

R, slant range = $\sqrt{x^2 + y^2 + z^2}$

δR, vector range = $xi + yj + zk$

x, y, z = position coordinates of a point

γ_x, γ_y, β = plane wave number components

In equation (47), the factor $e^{-iK \cdot \mathcal{R}}$ denotes a plane wave with the direction of the normal to the wave front given by the K vector. Also, since the source is at the origin, the plane wave has travelled through the distance given by $\mathcal{R}$. For a spherical wave, the radial direction vector is always perpendicular to the wave front, i.e., parallel to K, hence, the dot product is unnecessary in the exponent of the left hand side of equation (47).

Employing the geometry of figure 4, the field at P can be written in terms of the direct and reflected paths,

$$\Phi_p = \frac{1}{2\pi} \int_{-\infty}^{\infty}\int \frac{e^{-iK \cdot \mathcal{R}_1}}{i\beta} d\gamma_x \, d\gamma_y$$

$$+ \frac{1}{2\pi} \int_{-\infty}^{\infty}\int \frac{e^{-iK \cdot (\mathcal{R}_{2a} + \mathcal{R}_{2b})}}{i\beta} V(\alpha) \, d\gamma_x \, d\gamma_y \qquad (48)$$

where

$V(\alpha)$ = plane wave reflection coefficient

α = grazing angle

The reflection coefficient has been introduced in the second term of equation (48) in order to account for the reflection of the plane wave at the boundary between the half-spaces. By expanding the dot products, we can rewrite the two terms of equation (48) as follows,

$$\Phi_1 = \frac{1}{2\pi} \int_{-\infty}^{\infty}\int \frac{e^{-i(\gamma_x X + \gamma_y Y)} \, e^{-i\beta(z-d)}}{i\beta} d\gamma_x \, d\gamma_y \qquad (49)$$

$$\Phi_2 = \frac{1}{2\pi} \int_{-\infty}^{\infty}\int \frac{e^{-i(\gamma_x X + \gamma_y Y)} \, e^{-i\beta(z+d)}}{i\beta} V(\alpha) \, d\gamma_x \, d\gamma_y \qquad (50)$$

where

Φ_1 = potential for the direct path

Φ_2 = potential for the reflected path

Ingard[13] used this representation to summarize Weyl's work on the reflectivity of spherical waves; however, he adopted the angle of incidence to express the reflection coefficient and, subsequently, to transform the integral. In the work to follow, we will adopt the more common convention in underwater acoustics and employ the grazing angle, α.

In spite of the appearance of figure 4, the function Φ_2 includes the entire field resulting from the interaction of the incident wave with the lower half-space — not only the simple reflected wave. Inhomogeneous waves, for which β_1 is imaginary, are discussed in Appendix D and it is shown there that they are boundary waves travelling along the interface between the media. These waves

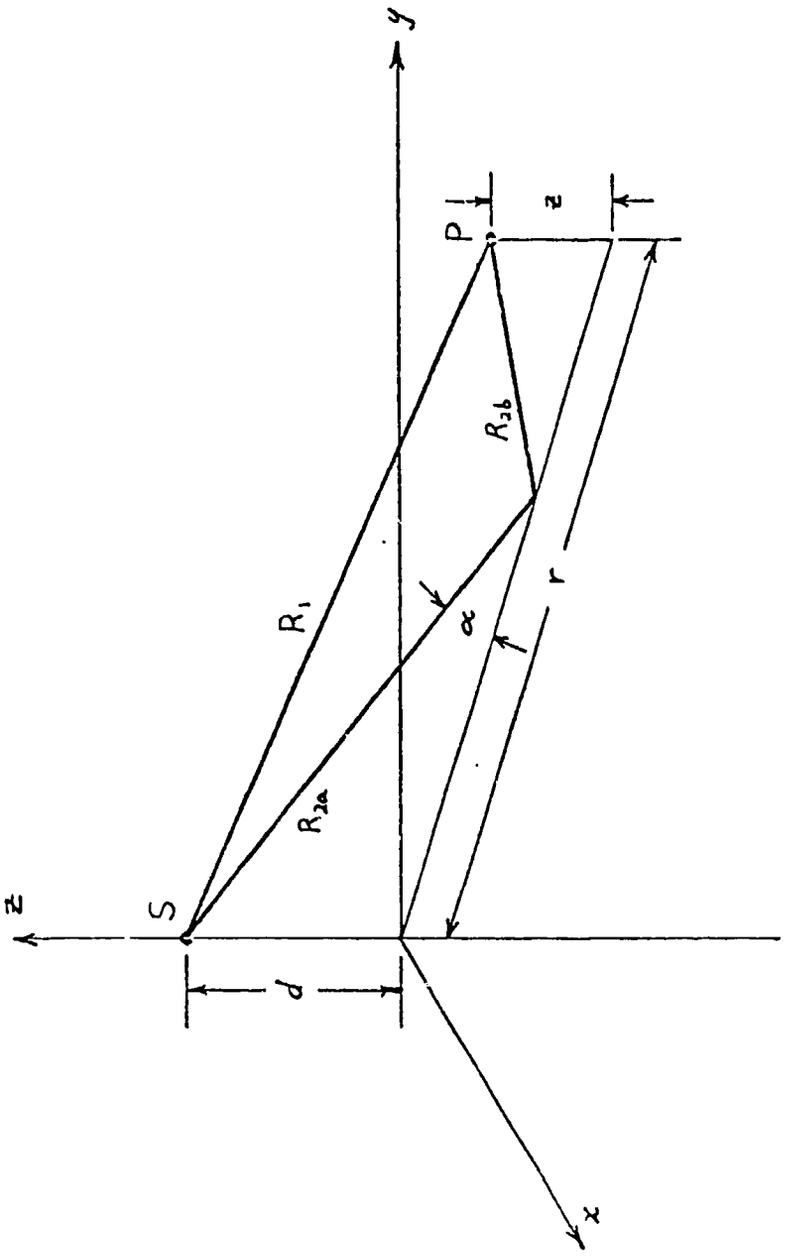

FIGURE 4. – Geometry of the two half-space problem. Paths shown are normals to the wavefronts of a direct (R_1) and a reflected (R_2) plane wave

are shown below to be included in equation (50). In order to investigate the behavior of this composite field, we will transform equation (50) by employing the geometry of the wave number vector. Figure 5 illustrates the relationship between the wave number, k, and the horizontal and vertical wave numbers, γ and β, and the grazing angle α. Observe in equation (47) that k describes the basic spherical wave we are attempting to reproduce and, therefore, is a constant. Thus, the extension of γ to infinity implies that β and α must become complex.

Following the same procedure illustrated in Appendix D to obtain equation (D-7), we transform equation (50) to an integration over γ,

$$\Phi_2 = \int_0^\infty J_0(\gamma r) \frac{e^{-i\beta_1(z+d)}}{i\beta_1} V(\alpha)\, \gamma\, d\gamma \tag{51}$$

In Appendix E, the solution for a homogeneous lower half-space is derived by solving the corresponding boundary value problem. If we compare equation (E-4) to equation (51), we observe that the two results are equivalent if the reflection coefficient is defined as,

$$V = \frac{\beta_1 - b\beta_2}{\beta_1 + b\beta_2} \tag{52}$$

This last result is, in fact, the plane wave reflection coefficient for the problem of two homogeneous half-spaces. A more familiar form of this result can be written in terms of the grazing angle α if we observe that, from figure 5,

$$\begin{aligned} \gamma &= k\cos\alpha = \frac{\omega}{c_1}\cos\alpha \\ \beta_1 &= k\sin\alpha = \frac{\omega}{c_1}\sin\alpha \end{aligned} \tag{53}$$

Introducing these last results and the definitions of β_1 and β_2 given in equations (18) into equation (52), the reflection coefficient expression becomes,

$$V(\alpha) = \frac{\sin\alpha - b\sqrt{\frac{c_1^2}{c_2^2} - \cos^2\alpha}}{\sin\alpha + b\sqrt{\frac{c_1^2}{c_2^2} - \cos^2\alpha}} \tag{54}$$

This last result is equivalent to that given by, for example, Clay and Medwin[14].

Equation (51) can now be transformed to the α-plane (the complex grazing angle plane) by writing the equivalent differential element from equation (53),

$$d\gamma = -k\sin\alpha\, d\alpha \tag{55}$$

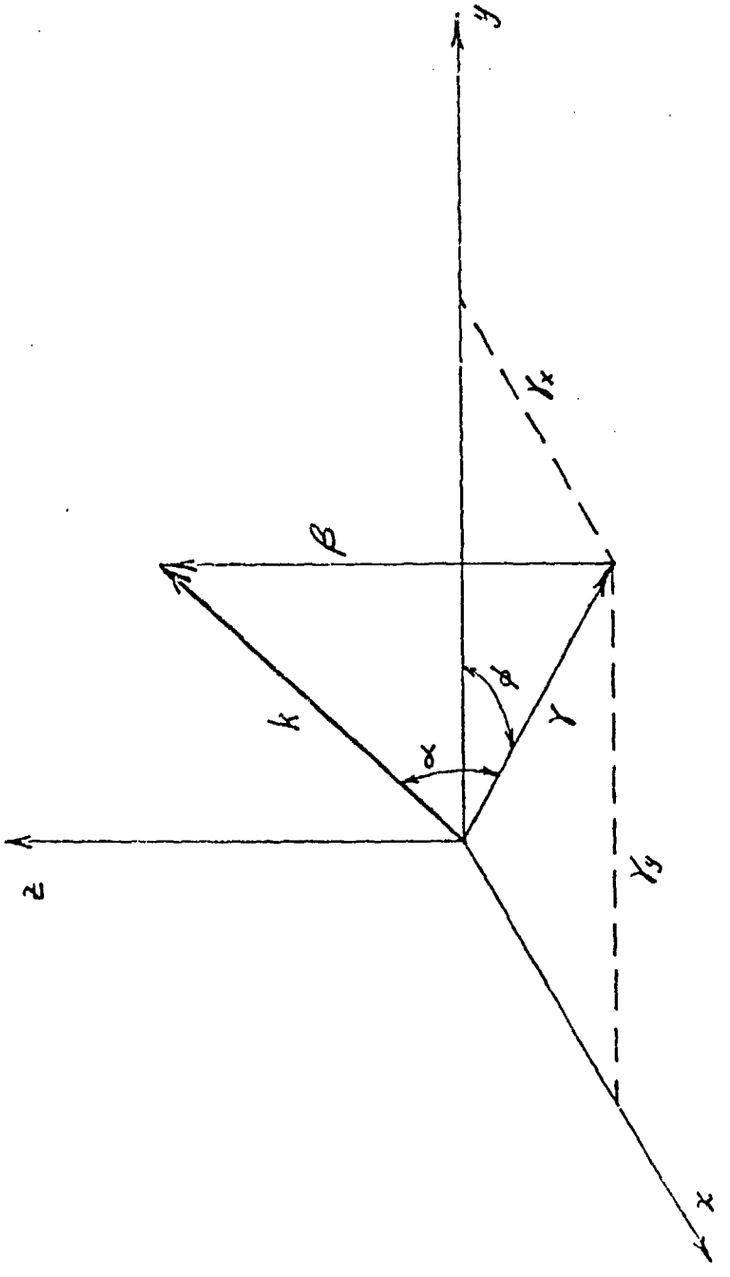

FIGURE 5. — Orientation and components of the wave number vector

To locate the path of integration in the α-plane, we write,

$$\begin{aligned}\gamma &= k \cos(\alpha' + i\alpha'') \\ &= k\,[\cos\alpha' \cosh\alpha'' - i \sin\alpha' \sinh\alpha'']\end{aligned} \tag{56}$$

where

α' = real part of α

α'' = imaginary part of α

Thus, it may be shown that,

$\gamma = -\infty$ for $\alpha' = \pi$ and $\alpha'' = \pm\infty$

$\gamma = 0$ for $\alpha' = \pi/2$ and $\alpha'' = 0$

$\gamma = +\infty$ for $\alpha' = 0$ and $\alpha'' = \pm\infty$

In order to insure that there is an exponential decay in the wave with increasing depth below the source, the imaginary part of β_1 must be negative; thus, from equations (53) we write,

$$\begin{aligned}\beta_1 &= k \sin(\alpha' + i\alpha'') \\ &= k\,[\sin\alpha' \cosh\alpha'' + i \cos\alpha' \sinh\alpha'']\end{aligned} \tag{57}$$

Therefore, when $\alpha' = \pi$, α'' must be positive and, if $\alpha' = 0$, α'' must be negative. Consequently, the transformed path of integration starts at $\alpha = \pi + i\infty$, moves down to $\alpha = \pi$, along the real axis to $\alpha = 0$, and ends at $\alpha = -i\infty$. This path is the reverse of path C in figure 6.

Applying these results to equation (51), the field integral becomes,

$$\Phi_2 = \frac{ik}{2} \int_{\pi + i\infty}^{-i\infty} H_0^{(2)}(kr\cos\alpha)\, e^{-ik(z+d)\sin\alpha}\, V(\alpha) \cos\alpha\, d\alpha$$

where

$H_0^{(2)}$ = Hankel function of the second kind.

Since the limits of integration can be interchanged, we obtain,

$$\Phi_2 = -\frac{ik}{2} \int_C H_0^{(2)}(kr\cos\alpha)\, e^{-ik(z+d)\sin\alpha}\, V(\alpha) \cos\alpha\, d\alpha \tag{58}$$

where

C = contour shown in figure 6.

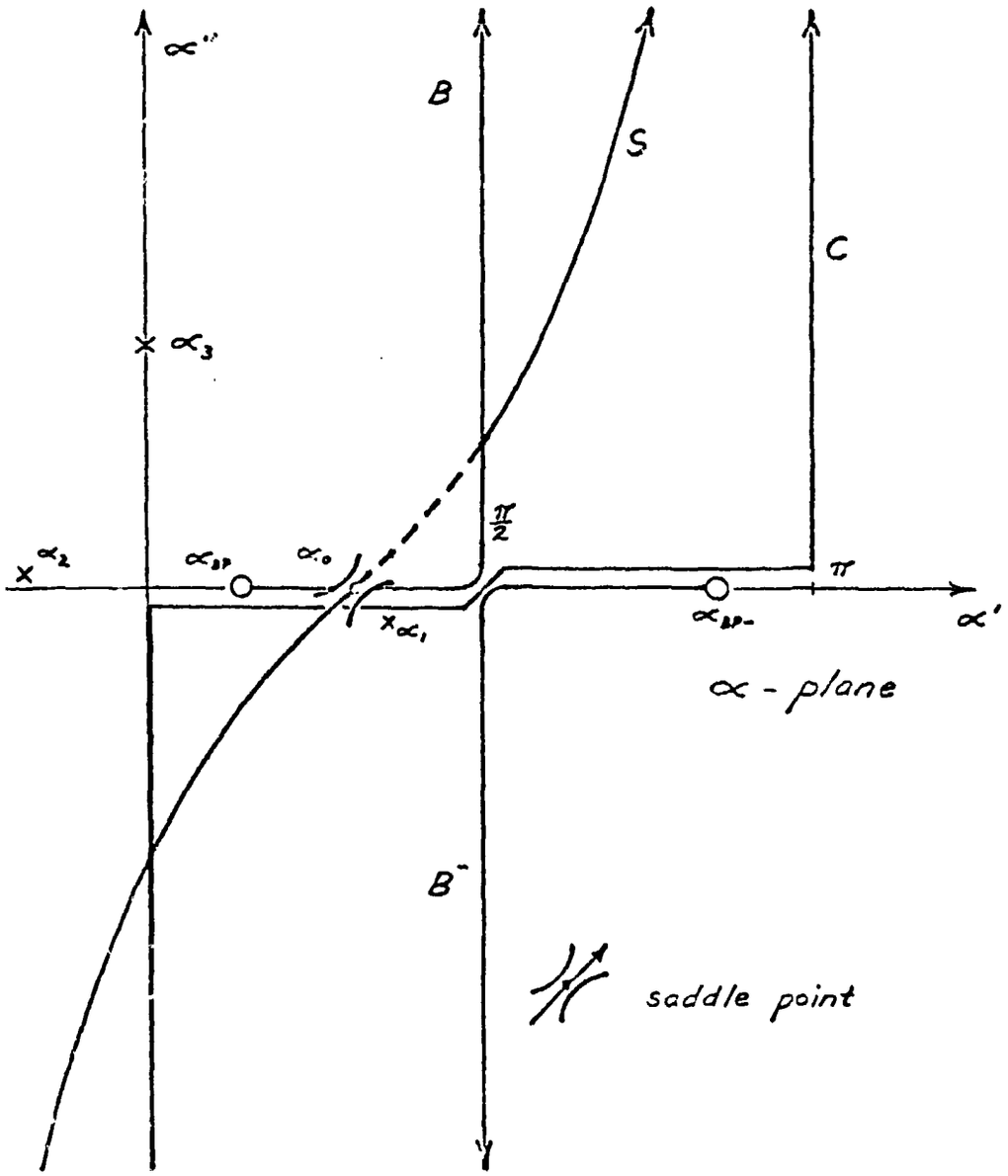

FIGURE 6. – Configuration of the complex grazing angle plane depicting the original integration contour C, the path of steepest descent, S, through the saddle point α_0, and the two branch lines, B and B^-

Asymptotic Expression for the Reflected Field

Equation (58) is the exact solution for the reflected field of figure 4; however, numerical evaluation of this expression is difficult because the integrand may oscillate very rapidly. Hence, we will consider an asymptotic approximation for the solution valid for large values of kr. This approximation is also useful for providing insight into the physical significance of the reflected field. In the following analysis, we will use procedures developed for electromagnetic wave propagation[15, 16], although our solution will be written in terms of the grazing angle rather than the angle of incidence.

First, the Hankel function is replaced by its asymptotic approximation and, in this case, we include the second term in the series expansion[9], hence,

$$H_o^{(2)}(kr\cos\alpha) \simeq \sqrt{\frac{2}{\pi kr\cos\alpha}}\left(1-\frac{1}{8ikr\cos\alpha}\right)e^{-i(kr\cos\alpha-\frac{\pi}{4})} \tag{59}$$

Combining the exponential factor indicated above with the exponential in equation (58), we obtain an exponential of the form,

$$e^{-ik\,[r\cos\alpha+(z+d)\sin\alpha]}$$

If we designate the length of path 2 in figure 4, i.e., the sum of R_{2a} and R_{2b}, by R and let the grazing angle shown be α_o, the above factor becomes,

$$e^{-ikR\cos(\alpha-\alpha_o)} \tag{60}$$

Introducing these changes into equation (58), we obtain,

$$\Phi_2 = e^{-i\frac{\pi}{4}}\sqrt{\frac{k}{2\pi r}}\int_C\left(1-\frac{1}{8ikr\cos\alpha}\right)e^{-ikR\cos(\alpha-\alpha_o)}\,V(\alpha)\sqrt{\cos\alpha}\,d\alpha \tag{61}$$

Next, we examine the characteristics of the integrand in the complex α-plane. There are three singularities of importance:

a) the two branch points of $V(\alpha)$, or, equation (54), given by,

$$\sqrt{\frac{c_1^2}{c_2^2}-\cos^2\alpha}=0$$

b) the poles of the function $V(\alpha)$, and,

c) the branch point located at

$$\sqrt{\cos\alpha}=0$$

Initially, let us consider the branch points of $V(\alpha)$,

$$\sqrt{\frac{c_1^2}{c_2^2}-\cos^2\alpha}=\frac{c_1}{\omega}\sqrt{\frac{\omega^2}{c_2^2}-\gamma^2}=\frac{c_1}{\omega}\beta_2=0 \tag{62}$$

These branch points and their associated branch cuts can be treated in the manner employed in the layered half-space problem. Referring to figure 3, we use the path equivalent of the EJP cut, i.e., the positive real axis in the β_2-place. Transformation of the EJP cut from the γ-plane to the α-plane yields path B in figure 6. Since there are two roots, α_{BP} and α_{BP_-}, to equation (62), a second branch cut must exist and it is shown as B^- in figure 6. Further, the branch is selected so that the imaginary part of $c_1\beta_2/\omega$ is negative; thus, the field decays with depth below the interface.

The poles of the function $V(\alpha)$ are determined by the zeroes of the denominator of equation (54), or,

$$\sin^2\alpha = b^2\left[\frac{c_1^2}{c_2^2} - \cos^2\alpha\right] \tag{63}$$

where

$\alpha = \alpha' + i\alpha''$

α' = real part of α

α'' = imaginary part of α

There are three roots to this last equation: two real roots, α_1 and α_2, and one imaginary root, α_3, as illustrated in figure 6. All of the poles resulting from these roots lie outside of the region defined by the contour integration; therefore, they can be ignored. Also, the branch point of $\sqrt{\cos\alpha}$ located at $\alpha = \pi/2$ can be avoided by drawing the contour C slightly above the point $\alpha = \pi/2$.

Since the behavior of the integrand of equation (61) has been established, we apply the method of steepest descent (or saddle point method) to approximate the integral solution. This method is discussed in detail in Appendix F. Basically, the technique involves locating the point at which the exponential of the integrand is stationary and then adjusting the path through this point so that the function decreases rapidly in magnitude on either side of the stationary point.

Consider an integral of the following form,

$$\int G(\alpha)\, e^{\rho f(\alpha)} d\alpha$$

Comparing this integral with equation (61), we conclude that,

$$\rho = kR \tag{64}$$

$$f(\alpha) = -i\cos(\alpha - \alpha_o) \tag{65}$$

$$G(\alpha) = e^{-i\frac{\pi}{4}}\sqrt{\frac{k}{2\pi r}}\left(1 - \frac{1}{8ikr\cos\alpha}\right) V(\alpha)\sqrt{\cos\alpha} \tag{66}$$

For large values of ρ, the magnitude of the exponential will be very sensitive to changes in $f(\alpha)$. Thus, proceeding as in Appendix F, the stationary point or saddle point of our function is located by utilizing equation (F-5) as follows,

$$\frac{df(\alpha)}{d\alpha} = i \sin(\alpha - \alpha_o) = 0$$

From this last result, we find that the stationary point is given by,

$$\alpha = \alpha_o$$

Hence, the major contribution of the reflected field comes from those plane waves which travel close to path R_2 in figure 4. Also, as discussed in Appendix F, the path of most rapid decrease in the real part of $f(\alpha)$ is the path of constant imaginary part; therefore, the phase is constant along this path. For this problem then, we will deform the contour of integration so that we are adding those plane waves that are close to the specularly reflected path and that arrive with identical phase.

From equation (F-6), the path of steepest descent is given by,

$$f(\alpha) = f(\alpha_o) - s^2$$

This last result can be written, employing equation (65), as,

$$\cos(\alpha - \alpha_o) = 1 - is^2 \tag{67}$$

The path described by equation (67) is shown in figure 6 as path S. As long as the saddle point α_o lies to the right of the branch point α_{BP}, the path crosses the branch cut B twice so that both ends of S lie on the proper branch. In this case, the original contour C can be deformed into S without any difficulty.

Physically, α_{BP} represents the critical angle of plane wave reflection theory. For grazing angles less than α_{BP}, the radical in equation (54) becomes imaginary and the magnitude of $V(\alpha)$ is unity; thus, the plane wave is totally reflected. If the grazing angle of the plane wave is greater than α_{BP}, the wave is only partially reflected. In the following analysis, the asymptotic solution to equation (61) will completely describe the field only if the angle shown in figure 4 is greater than the critical angle. As point P in figure 4 moves outward, the angle will pass through the critical angle and, from this point on, another term will appear in the solution. This term, a result of the branch line integral associated with α_{BP}, will be considered later.

The asymptotic solution to equation (61) can be written by substituting equations (64), (65) and (66) into equations (F-10), (F-14) and (F-15). Neglecting terms of the order, $1/(kr)^2$, the reflected field is given by,

$$\Phi_2 = \frac{e^{-ikR}}{R} \left\{ V(\alpha_o) + \frac{i}{2kR} \left[V''(\alpha_o) - V'(\alpha_o) \tan \alpha_o \right] \right\} \tag{68}$$

where

$kR >> 1.$

If we had only considered the first term, we would have obtained the field resulting from a single plane wave following path 2 in figure 4. Indeed, for large kR, the second term of equation (68) can be ignored and the problem can be treated by applying the plane wave reflection coefficient directly to the spherical wave incident at the boundary between the media. The second term of the solution provides a correction for the plane wave reflection coefficient when the incident wave is spherical. Finally, the validity of equation (68) depends not only on kR being large, but also on $V(\alpha)$ being a slowly varying function. In the derivation of the method of steepest descent, it was assumed that the exponential factor, equation (60), decreased in magnitude so rapidly on either side of the saddle point that the remainder of the integrand given by equation (66) could be adequately represented by the first few terms of its Taylor series. As can be shown from equation (54), the reflection coefficient $V(\alpha)$ varies rapidly in the vicinity of the critical angle; hence, equation (68) is not accurate for α_o approximately equal to α_{BP}, the critical angle.

Lateral Wave

When the grazing angle α_o of figure 4 is less than the critical angle α_{BP}, the path of steepest descent no longer crosses the branch cut twice. Consequently, a circuit around the branch cut must be added to insure that the path closes on the same branch as the original contour. Figure 7 illustrates this modified contour. The branch line integral introduced into the solution corresponds to another form of energy propagation which we will now consider.

Only the reflection coefficient $V(\alpha)$ changes value in crossing the branch cut; thus, the exponential factor of the branch line integrand is identical to that in equation (61). By introducing a modification to the method of steepest descent, we can evaluate this branch line integral asymptotically. Brekhovskikh[16] outlined this modification and obtained a complete solution; however, we will only follow his work to the point of locating the path of descent. Once the proper path has been found, it will be transformed back to the γ-plane so that the results can be applied to the layered half-space problem. Since the branch cut must originate from the branch point, we are not able to deform the path as freely as in the case of contour C, figure 7. We can, however, locate the path leading away from α_{BP} over which the function decreases most rapidly. Under these circumstances, most of the contribution to the integral comes from the immediate vicinity of α_{BP} and we can approximate the integrand by a series similar to that derived in Appendix F. In the saddle point method, we locate the saddle of the function, then descend along the steepest path into the valleys on either side of the saddle. In the present case, our starting point is located somewhere on the ridge flank or valley wall and we descend along the steepest path into the nearest valley.

The real part of $f(\alpha)$ decreases most rapidly along the desired path; therefore, as shown in Appendix F, the imaginary part is constant. As a result, the path of descent is given by,

$$f(\alpha) = f(\alpha_{BP}) - s \quad (0 < s < \infty) \tag{69}$$

We can show that this path leaves α_{BP} with a vertical slope and approaches the upper leg of S (see figure 7) asymptotically. Figure 8 illustrates the branch line integral path BLI and the steepest descent deformation B_a after transformation to the complex γ-plane. Also shown is the transformed saddle point γ_o with its associated descent path S.

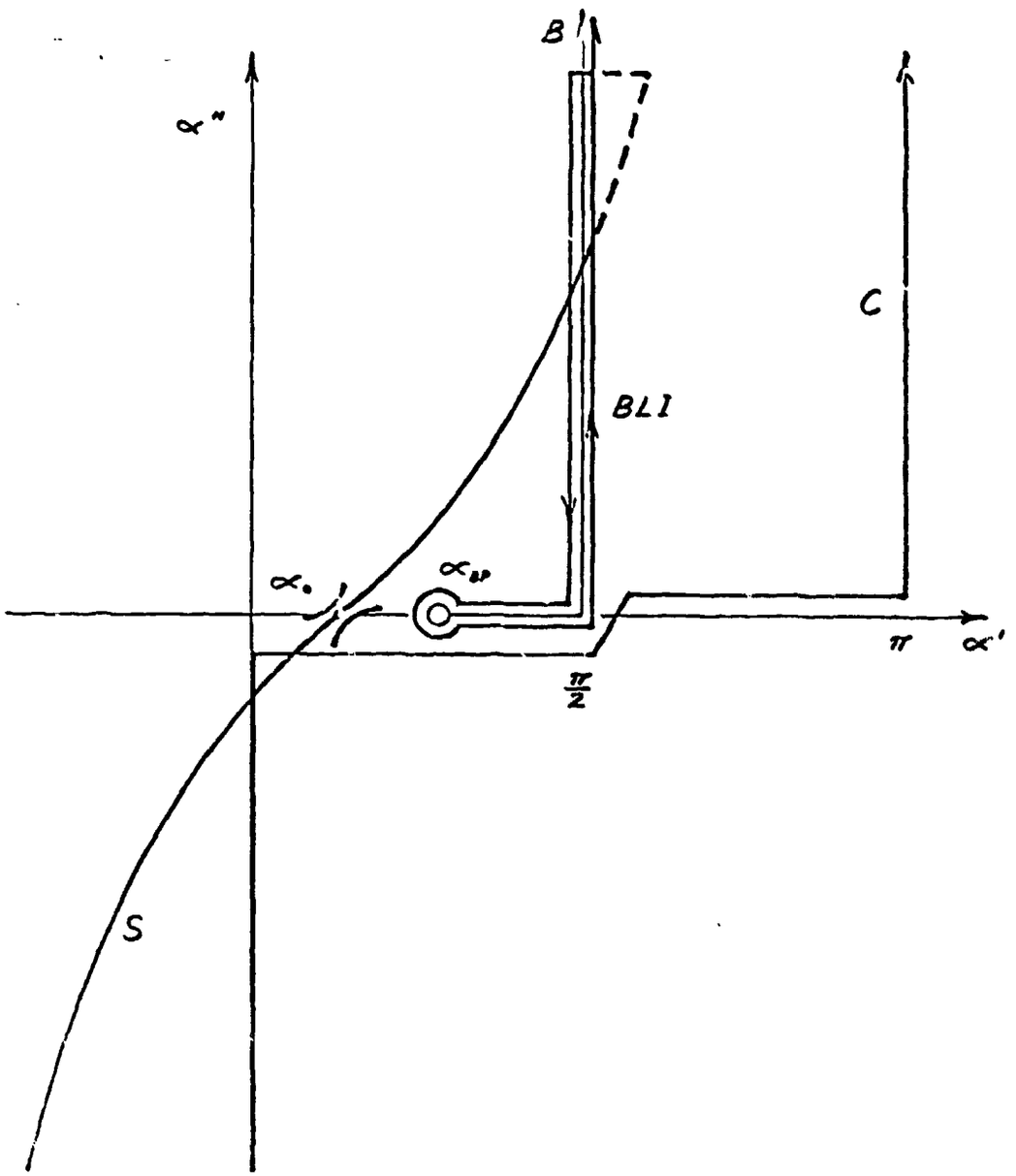

FIGURE 7. – Modification of path of steepest descent, S, for $\alpha_0 < \alpha_{BP}$. Inclusion of branch line integral, BLI, restores upper end of S to same branch as original contour, C

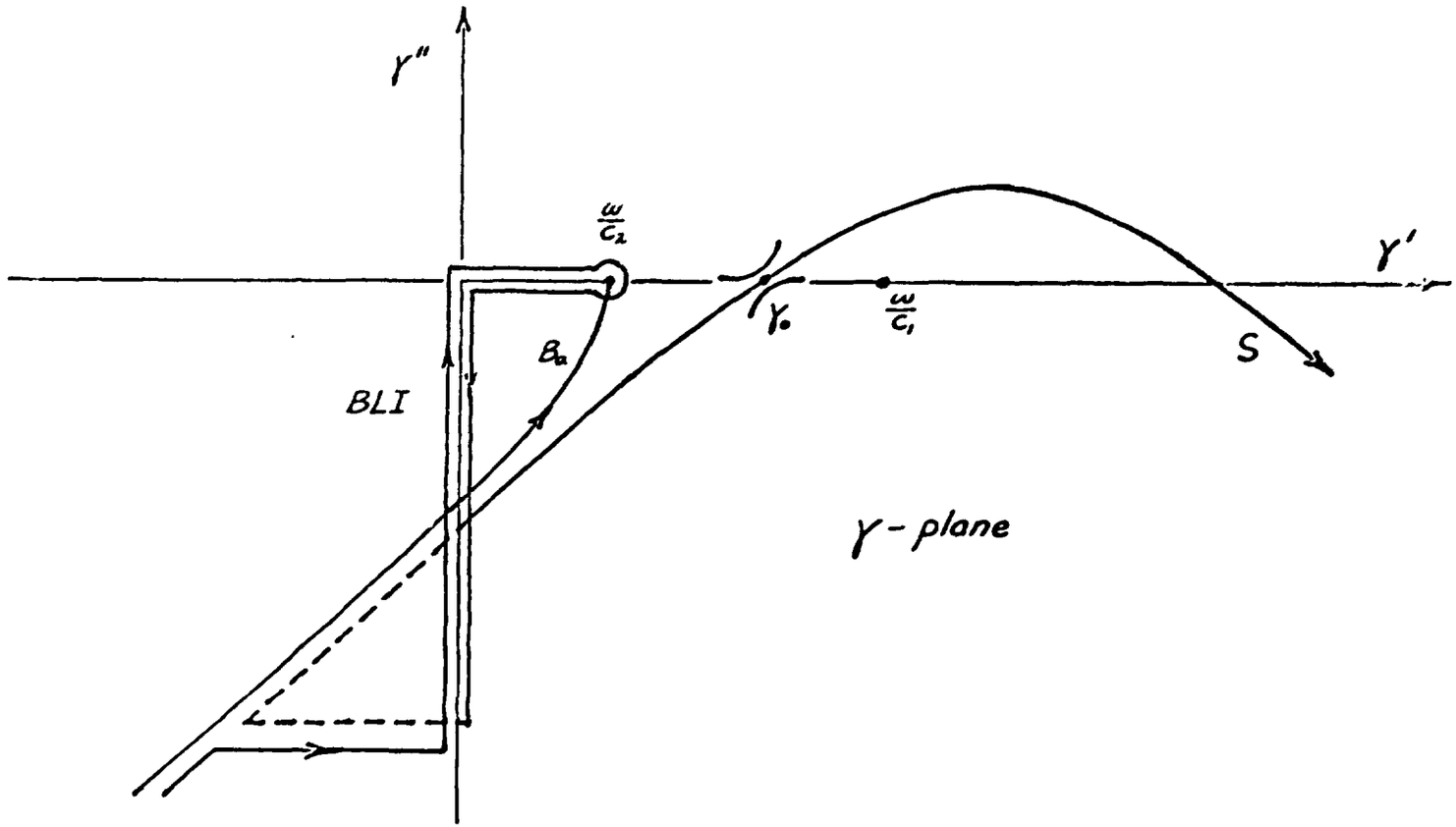

FIGURE 8 - Path of steepest descent, S, and branch line integral, BLI, transformed to γ-plane. Also depicted is the path, B_a, for asymptotic evaluation of the branch line integral

Using equations (51) and (52), we can express the branch line integral over the path BLI as follows,

$$\Phi_B = -\frac{1}{2} \int_{-i\infty}^{\frac{\omega}{c_2}} H_o^{(2)}(\gamma r) \frac{e^{-i\beta_1(z+d)}}{i\beta_1} \left[\frac{4b\beta_1\beta_2}{\beta_1^2 - b^2\beta_2^2}\right] \gamma d\gamma$$

Note that in the above integral the usual replacement of J_o by $H_o^{(2)}$ has been performed. From figures 6 and 7, we note that no poles are crossed in the process of deforming the branch cut so that the solution can be written directly by changing the path,

$$\Phi_B = 2bi \int_{B_a} H_o^{(2)}(\gamma r)\, e^{-i\beta_1(z+d)} \left[\frac{\beta_2}{\beta_1^2 - b^2\beta_2^2}\right] \gamma d\gamma$$

If the asymptotic form for the Hankel function is used, the above expression reduces to,

$$\Phi_B = 2ibe^{i\frac{\pi}{4}} \sqrt{\frac{2}{\pi r}} \int_{B_a} e^{-i[\gamma r + \beta_1(z+d)]} \left[\frac{\beta_2}{\beta_1^2 - b^2\beta_2^2}\right] \sqrt{\gamma}\, d\gamma \qquad (70)$$

Since the descent path, B_a, is initially vertical downward and only the beginning of the path contributes significantly to the integral, we can assume that the real part of γ does not change. In other words, γ is given by,

$$\gamma \simeq k_2(1 - ix) \qquad (71)$$

where x is small in the region of interest.

In view of this last conclusion, we write the following approximations,

$$\gamma^2 \simeq k_2^2(1 - 2ix)$$

$$\beta_2 = \sqrt{k_2^2 - \gamma^2} \simeq k_2\sqrt{2ix}$$

$$\beta_1 = \sqrt{k_1^2 - \gamma^2} \simeq k_1\sqrt{1 - \frac{c_1^2}{c_2^2}} \qquad (72)$$

$$\beta_1^2 - b^2\beta_2^2 \simeq \beta_1^2$$

$$d\gamma \simeq -ik_2 dx$$

After substituting these approximations into equation (70) and transforming the integral to an integration over x^{17}, the field can be written as,

$$\Phi_B = \frac{-4ibk_2^{5/2}}{\beta_1^2\sqrt{\pi r}}\, e^{-i[k_2 r + \beta_1 (z+d)]} \int_0^\infty \sqrt{x}\, e^{-k_2 r x}\, dx$$

The integration may now be performed and the final result is,

$$\Phi_B = \frac{-2ibk_2}{\beta_1^2 r^2}\, e^{-i[k_2 r + \beta_1 (z+d)]} \tag{73}$$

where β_1 is given by equations (72).

In order to establish the physical significance of the solution, consider the exponential factor of equation (73). By employing the definition of the critical angle, equation (62), and the geometry of figure 9, we can write equation (73) in the following form,

$$\Phi_B = \frac{-2ibk_2}{\beta_1^2 r^2}\, e^{-ik_2 (r - R_2 \cos \alpha_{BP})}\, e^{-ik_1 R_2} \tag{74}$$

The second exponential factor indicates that the energy associated with the wave travels along the path with grazing angle, α_{BP}, regardless of the range. Moreover, as shown in figure 9, the two legs of this path, the incident and reflected segments, are separated by a horizontal portion equal to the range excess over the minimum range, $R_2 \cos \alpha_{BP}$. Since the wave number is k_2 for this horizontal segment, the speed of propagation along the interface is c_2. Not only is the path of this wave significantly different from the direct and specularly reflected paths (refer to figure 4): according to equation (74) the amplitude decreases as r^{-2}. We observe that this is a much more rapid decrease than the r^{-1} decrease associated with spherical spreading. Furthermore, the shape of the wavefront is a straight line in the rz space, i.e., a conic section in cylindrical space, as is seen by allowing the exponent of equation (73) to assume a constant value,

$$k_2 r + k_1 \sqrt{1 - \frac{c_1^2}{c_2^2}}\, (z+d) = \text{const.}$$

The line of constant phase (the wavefront) is given by,

$$z = \frac{-r}{\tan \alpha_{BP}} + \text{const.}$$

In contrast, we note that, from equation (68), the wavefront of the reflected wave (and, incidentally, the direct wave) is a circle,

$$R^2 = r^2 + (z+d)^2 = \text{const.}$$

This, of course, would be the section of a sphere in three dimensions.

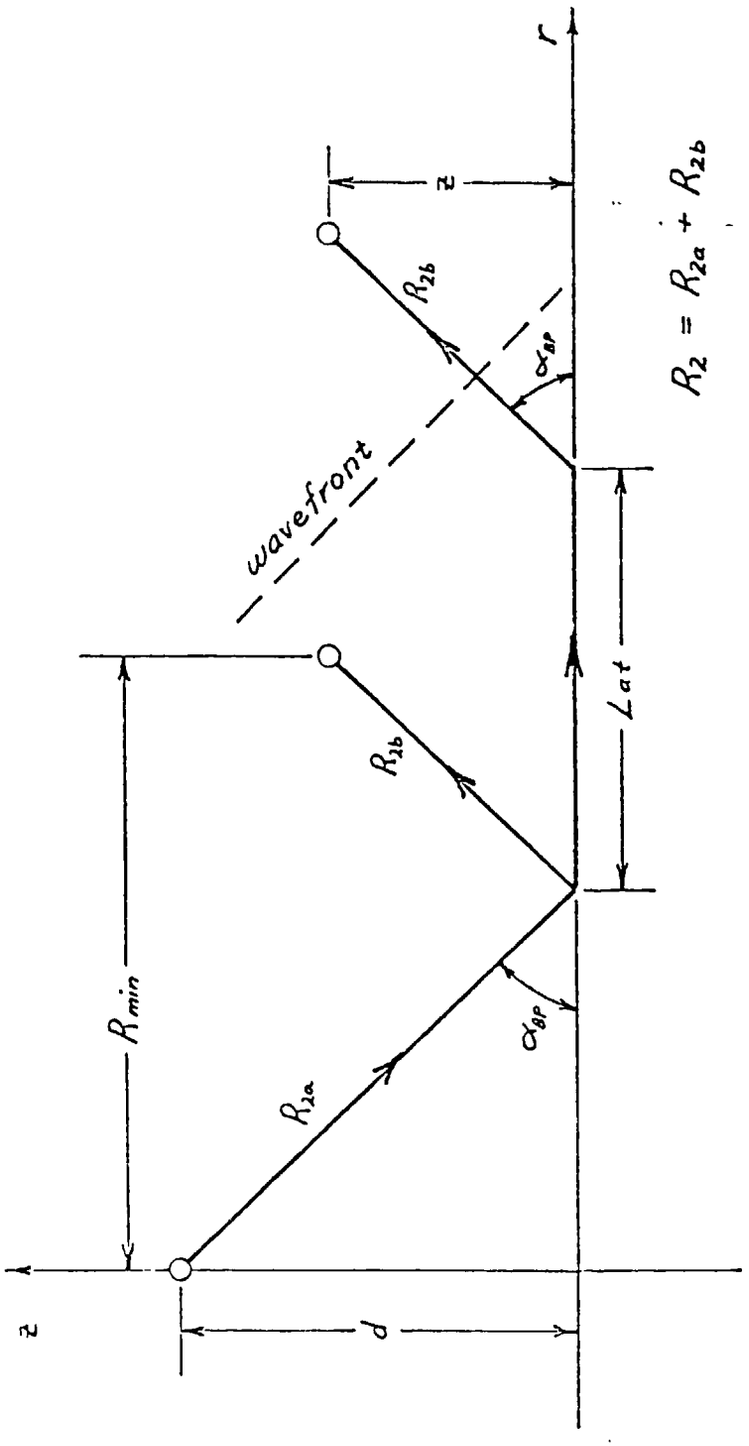

FIGURE 9. — Onset of the lateral wave at range greater than $R_{min} = R_2 \cos \alpha_{BP}$. Horizontal displacement, Lat, and wavefront are also shown.

Layered Half-Space Branch Line Integral

Now that we have developed the concept of a lateral wave, we can return to the finite layer problem and discuss the original branch line integral, equation (44). Unfortunately, the problem is more complex and, thus, we will be forced to introduce some additional assumptions.

By employing the asymptotic form of the Hankel function, equation (44) can be simplified as follows,

$$\Phi_B = -\sqrt{\frac{2}{\pi r}}\, e^{i\frac{\pi}{4}} \int_{\frac{\omega}{c_2}}^{\frac{\omega}{c_2}-\infty} e^{-i\gamma r}\sqrt{\gamma}\,[G(\beta_1,\beta_2) - G(\beta_1,-\beta_2)]\, d\gamma \qquad (75)$$

This last result may appear to be in a form suitable for the method of steepest descent; however, there are additional exponential terms to be considered. These additional terms arise from the function G in equation (75). If we replace the sine and cosine functions in equation (30), the equation that defines G, with complex exponentials and perform the indicated operations we can write,

$$\begin{aligned} G(\beta_1,\beta_2) = \frac{1}{2i\beta_1}\Big\{ & e^{-\beta_1(z-d)} - e^{-i\beta_1(z+d)} \\ & -V\left[e^{-i\beta_1(2H+z-d)} - e^{-i\beta_1(2H+z+d)} - e^{-i\beta_1(2H-z-d)} + e^{-i\beta_1(2H-z+d)}\right] \\ & +V^2\left[e^{-i\beta_1(4H+z-d)} - e^{-i\beta_1(4H+z+d)} - e^{-i\beta_1(4H-z-d)} + e^{-i\beta_1(4H-z+d)}\right] \\ & -V^3[\quad] + \ldots \end{aligned} \qquad (76)$$

where V = reflection coefficient defined by equation (52).

In the same manner, we discover that the expression for $G(\beta_1, -\beta_2)$ is identical with equation (76) with the exception that β_1 is replaced by $-\beta_1$.

Before proceeding further, it is interesting to examine the nature of the terms in equation (76). Each of the terms, when combined with the exponential from the asymptotic form of the Hankel function assumes the following form,

$$e^{-iK\cdot\Re}$$

where

K, vector wave number = $\gamma r + \beta_1 k$

$\Re$, position vector = $rr \pm (2nH \pm z \pm d)\,k$

After integration over the horizontal wave number γ, this expression corresponds to the field of a spherical wave (see Appendix A) at the point given by the position vector $\Re$. Figure 10 illustrates the correspondence of each term to a spherical wave at an image receiver located so as to produce the required number of surface and bottom reflections. Thus, we have shown that equation (24), the general field solution in the layer, can be thought of as a superposition of spherical waves travelling along the various direct and reflected paths from source to observation point[2].

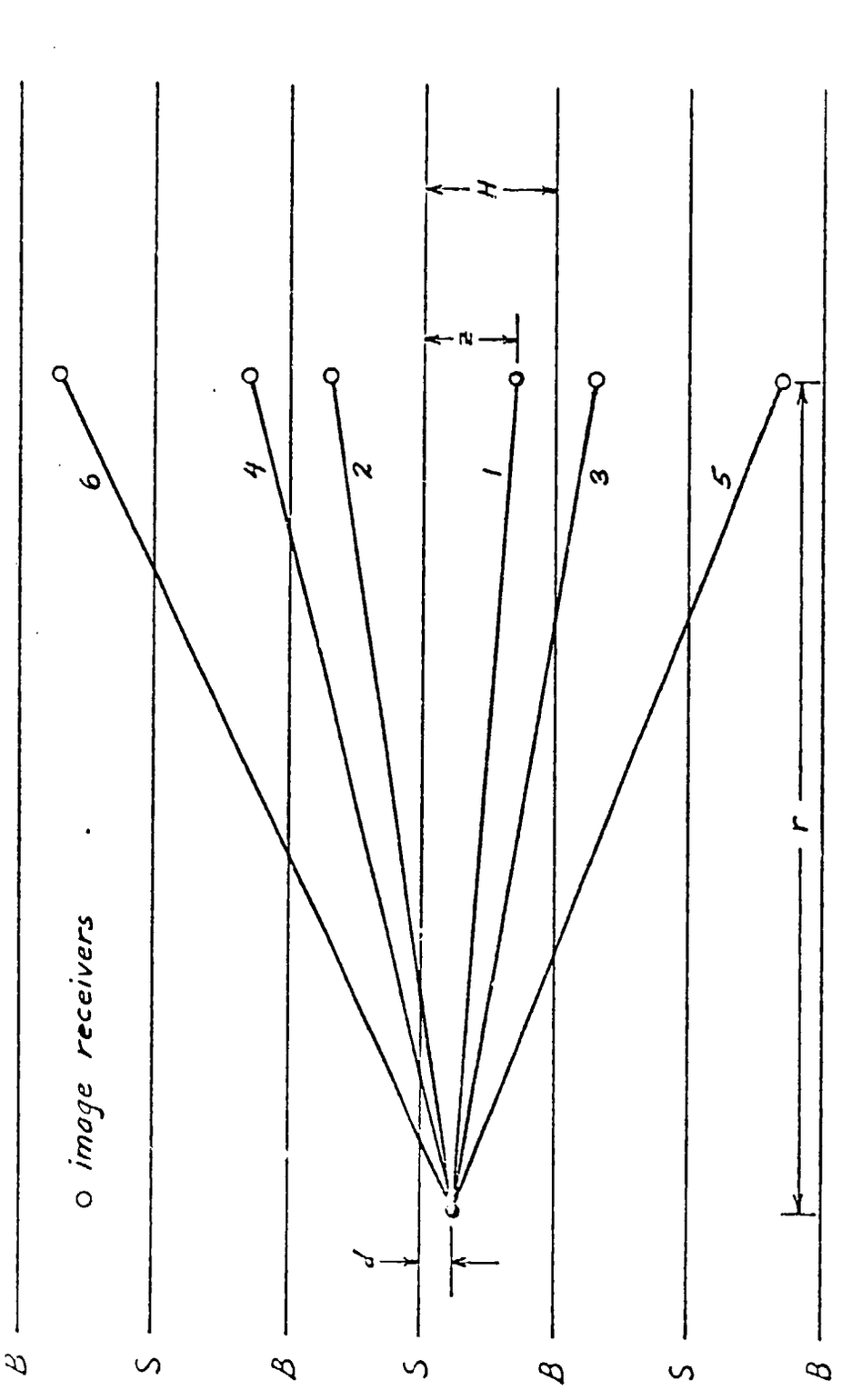

FIGURE 10. – Multiple paths from source to receiver illustrated by layer images. Surface and bottom images planes are denoted S and B respectively.

Strictly speaking, in order to apply the method of steepest descent to equation (75), we must consider a separate path for each term in equation (76) and its counterpart for $G(\beta_1, -\beta_2)$. Instead of following such a difficult course, we introduce three assumptions to insure that the problem is tractable. First, consider the leakage of waves into the half-space for grazing angles greater than the critical angle to be significant. This appears to be a reasonable assumption in many cases and allows the neglect of terms multiplied by powers of the reflection coefficient V. Further, we shall assume that the range is much greater than the largest value of $2nH + z + d$ in the remaining terms so that the variation of the exponential factor in equation (75) dominates the integrand. Under these restrictions, we shall consider the path of steepest descent required by the function,

$$e^{-i\gamma r}$$

In this case, the descent path is the Pekeris branch line path and, therefore, the approximations given by equations (72) can be used. Notice that this path is valid for either the EJP branch line integral or the Pekeris integral; however, in order to deform the EJP contour into the descent path, all of the poles in the Pekeris solution that are crossed must be accounted for as residues.

Finally, there is one more restriction on the approximation we are about to make. The method of steepest descent, in its present form, breaks down when a pole is located near the saddle point or the descent point. This circumstance is a possibility in the layered half-space problem. Whenever a mode approaches cut-off, i.e., the transition between trapped and leaky waves, the pole associated with the mode approaches the branch point. Cutoff is determined by the characteristic equation for the poles, equation (33), which can be written,

$$\tan \beta_1 H = \frac{-\beta_1}{b \sqrt{\omega^2 \left(\frac{1}{c_1^2} - \frac{1}{c_2^2} \right) - \beta_1^2}}$$

At the branch point $\gamma = \omega/c_2$, and, consequently, the right side of the above equation becomes infinite. In order for a root to exist at the branch point, the left side must also be infinite or,

$$\beta_1 H \Big|_{\gamma = \omega/c_2} = \frac{\omega H}{c_1} \sqrt{1 - \frac{c_1^2}{c_2^2}} = \frac{(2n-1)\,\pi}{2} \tag{77}$$

This is the condition for cutoff of the n^{th} mode. We must not use the approximation developed below when equation (77) is satisfied for any positive integer value of n.

Now that we have outlined the restrictions in our theory, we may apply the approximations indicated in equations (72) to determine the value of equation (75). In addition to equations (72), we observe that,

$$\beta_1^2 \cos^2 \beta_1 H + b^2 \beta_2^2 \sin^2 \beta_1 H \simeq \beta_1^2 \cos^2 \beta_1 H \tag{78}$$

provided that $\cos \beta_1 H \neq 0$, since β_2 is much less than β_1. This condition is equivalent to requiring that no modes are near cutoff.

Substituting the above approximation, equation (78), and equations (72) in equation (75), we can show that,

$$\Phi_B \simeq \frac{4ibk_2^3 \sin\beta_1 d \sin\beta_1 z}{\sqrt{k_2}\,\beta_1^2 \cos^2\beta_1 H \sqrt{\pi r}}\, e^{-ik_2 r} \int_0^\infty \sqrt{x}\, e^{-k_2 x r}\, dx$$

As in the derivation of equation (73), this integral can be evaluated; hence, the asymptotic field resulting from the branch line integral is,

$$\Phi_B = \frac{2ibk_2 \sin\beta_1 d \sin\beta_1 z}{r^2 \beta_1^2 \cos^2\beta_1 H}\, e^{-ik_2 r} \tag{79}$$

In this last result, β_1 is evaluated at $\gamma = \omega/c_2$.

As in the case of the lateral wave in the two half-space problem, this field exhibits a spreading loss of $1/r^2$. Also, by examining the exponent of equation (79), we see that the phase velocity of this wave is equal to the sound speed in the half-space below the layer. Since we have assumed that the horizontal range is considerably larger than the water depth, the two legs of the lateral wave's path away from the interface are so small that their effects are not evident in equation (79).

Application to a Shallow Water Waveguide

In order to illustrate the behavior of the field in a fluid layer, a specific example will be considered. The following values were selected for the parameters in figure 1 in an attempt to describe a region of shallow water over a fluid sediment of moderate reflectivity:

$b = \rho_1/\rho_2 = 0.5$
$C_1 = 1500$ m/sec
$C_2 = 1600$ m/sec
$d = 20$ m
$H = 50$ m
$z = 40$ m

Below cutoff for the first mode (21.55 Hz) the field was determined by numerical integration of equation (24). For higher frequencies, poles appear on the real axis, representing trapped modes, and the integration becomes extremely difficult. Hence, above cutoff, the field was evaluated by summing the residues of the real poles and numerically integrating the EJP branch line integral given by equation (46). In this manner, it was not necessary to locate the complex poles. Finally, the lateral wave field was computed separately by numerical integration of the Pekeris branch line integral. equation (44). Each of the numerical integration computer programs was patterned after the algorithm described by Bucker[12] which is a Guass-quadrature scheme with adaptive step size.

Figures 11, 12 and 13 illustrate the changes in the field as the source frequency is increased. Propagation loss, plotted as a function of range, refers to the ratio of intensity (proportional to pressure squared) at the observation point to the intensity one meter from the source. In decibel form this ratio is simply $20 \log|\Phi|$ since the intensity at one meter was defined as unity by the left side of equation (A-5).

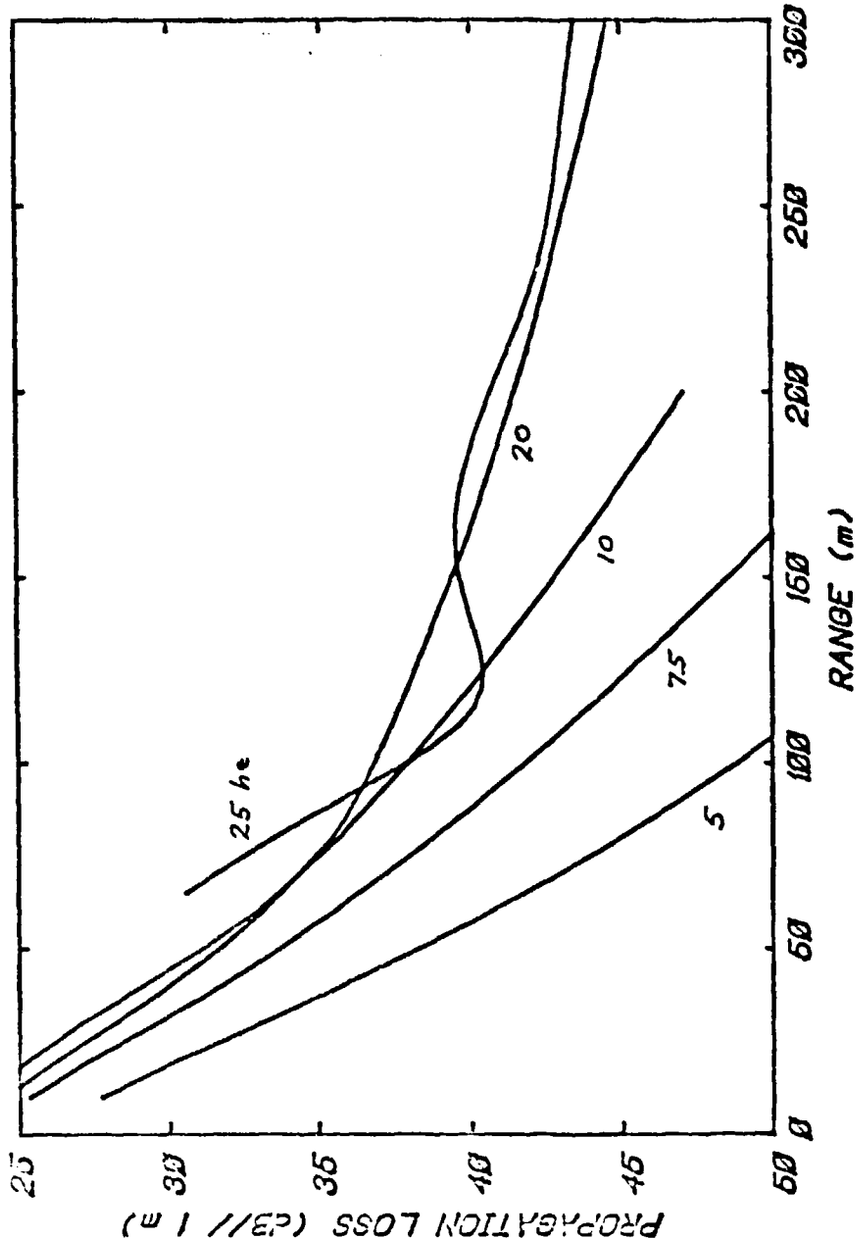

FIGURE 11. — Propagation loss in a shallow water waveguide for frequencies up to and slightly above first mode cutoff (21.55 Hz)

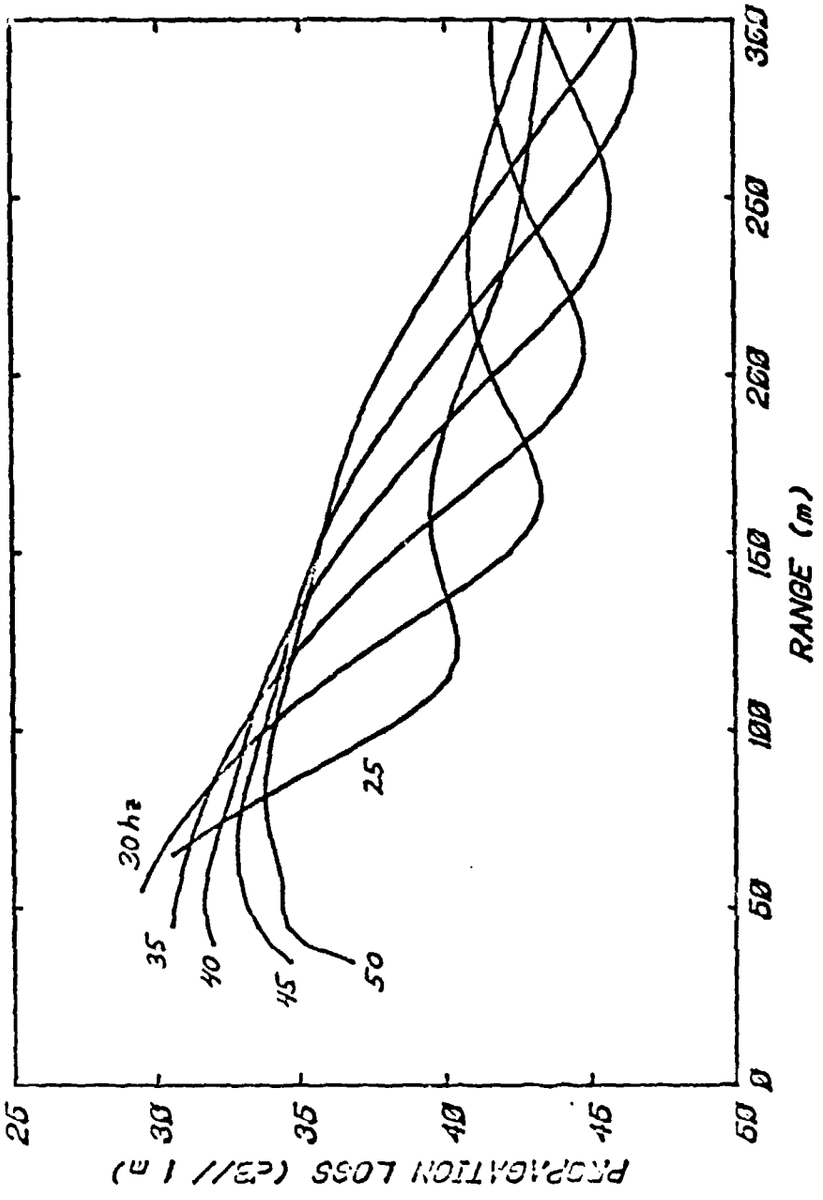

FIGURE 12. — Propagation loss for only one trapped mode

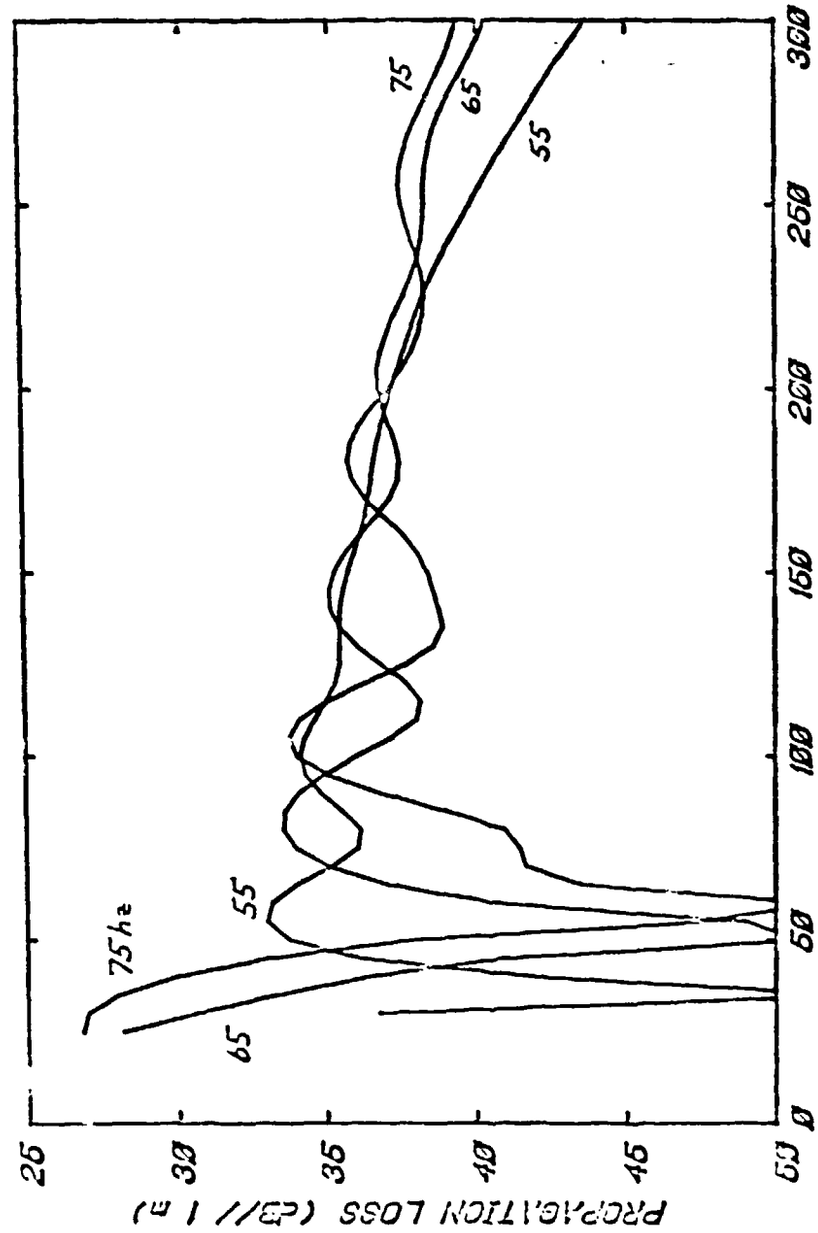

FIGURE 13. – Propagation loss for frequencies bounding cutoff of second mode (64.66 Hz)

In figure 11, the 5 Hz curve shows a rapid attenuation of the field with range. This behavior is typical of a waveguide well below cutoff. As the frequency increases, the curves remain smooth and indicate that the field decays less rapidly. Above cutoff, that is, above 21.55 Hz, the appearance of the first trapped mode induces oscillations as shown by the 25 Hz curve. Referring to figures 12 and 13, we observe that the oscillations retain a similar form from 25 Hz to 60 Hz. Effects of the second trapped mode, which appears above 64.66 Hz, are clearly evident as distortions in the oscillations of the 75 Hz curve. Generally, as more trapped modes appear, the shape of the curve becomes increasingly complex.

Another significant component of the field is the contribution of the lateral wave as given by the Pekeris branch line integral. This component is plotted in figures 14 and 15 illustrating the smooth decay with range at all frequencies. Of particular importance are the curves at 20 Hz and 65 Hz which are substantially higher in level than any of the other curves. Since the frequencies associated with these curves correspond roughly to the cutoff frequencies of the first and second modes, we conclude that the lateral wave is strongly excited when a mode is near cutoff. In fact, at 20 Hz, the lateral wave is the predominant field component (compare figures 11 and 14) and this explains the relatively slow decay with range although, at 20 Hz, the layer supports no trapped modes.

This behavior of the lateral wave when a mode is near cutoff is reasonable both mathematically and physically. Mathematically, a mode near cutoff implies that a pole is close to the starting point of the branch line; therefore, the value of the integral is large. Incidentally, the proximity of the pole to k_2 renders the asymptotic solution, equation (79), invalid. In fact, the approximate integration considerably overestimates the field in this case. Physically, a pole near k_2 reflects the existence of a mode whose wavefront normal is close to the critical angle at the interface. From our analysis of the two half-space problem and figure 9, we observe that this is the preferred direction for the interface wave in the upper medium.

One final note concerning the data presented in figures 11 through 15 is necessary. Numerical integration of the Pekeris and EJP branch line integrals was performed by employing the asymptotic form of the Hankel function. As a consequence, the curves have been constructed so that the argument, γr, of each Hankel function is at least 2π. Below cutoff, the computation utilized a polynomial approximation to the Bessel function valid over the entire range of the Bessel function argument.

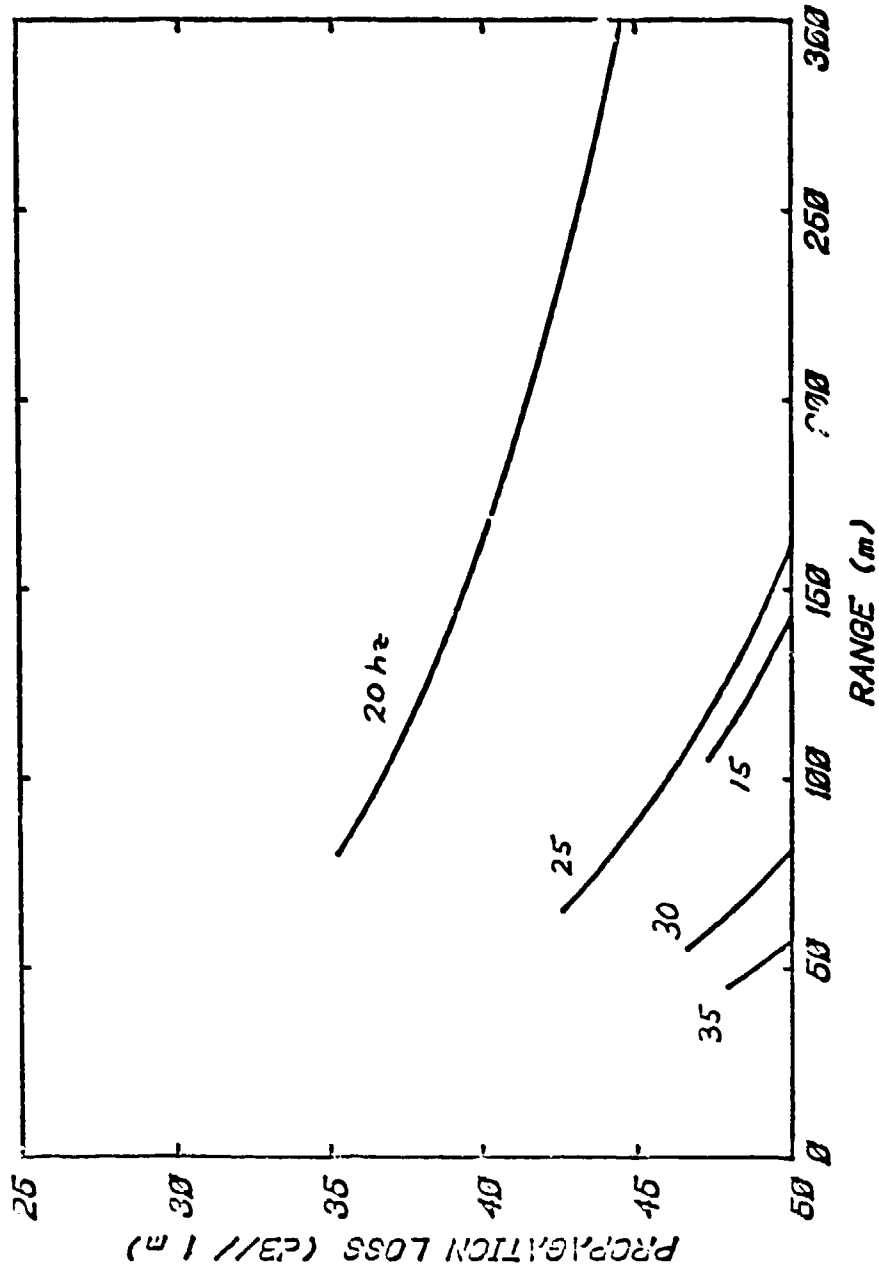

FIGURE 14. — Lateral wave contribution showing excitation peak near cutoff of first mode (20 Hz curve)

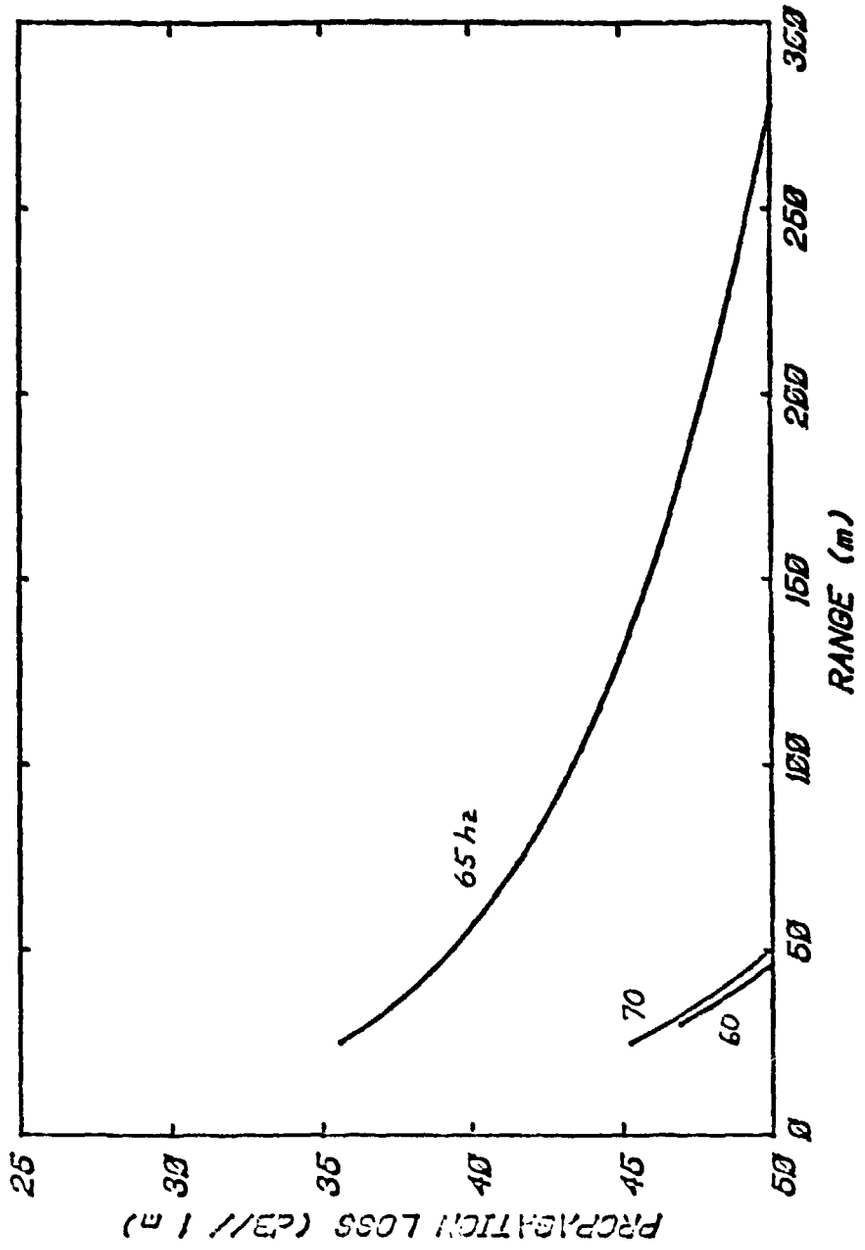

FIGURE 15. – Lateral wave contribution showing excitation peak near cutoff of second mode (65 Hz curve)

CONCLUSIONS

The boundary value problem for a point harmonic source in a layer of fluid over a fluid half-space has been solved by superposition of elementary wave functions and contour integration in the complex wave number plane. Three different forms of this solution have been determined. Specifically, these are: (1) the basic superposition integral given by equations (23) through (25); (2) a finite sum of real mode residues, equation (35), and the EJP branch line integral given by equation (46); and (3) a finite sum of real modes, an infinite sum of complex modes and the Pekeris branch line integral, equation (45). All of these solutions are mathematically equivalent; however, each has its own particular advantages.

Direct numerical integration of the superposition integral is straightforward provided that the layer is below cutoff. In the event that trapped modes exist, there will be poles on the real axis and, as the frequency increases, the integrand becomes increasingly oscillatory. As a result, the numerical integration becomes difficult. On the other hand, poles on the real axis are simple to locate by means of the characteristic equation, equation (33); hence, their contribution to the field is simple to compute. In this case, the EJP integral must also be evaluated and this evaluation is frequently difficult because the integrand can oscillate rapidly. However, we observe that the envelope of these oscillations tends to have a finite number of large but narrow peaks and these may be individually approximated by analytical functions and integrated. Known as virtual modes or resonances, the contributions from these peaks correspond in behavior to the lower order leaky modes [18,19,20]. The concept of virtual modes represents an approximation to the EJP integral and yields a physical interpretation in terms of leaky modes of propagation.

In comparison with the EJP integral, the Pekeris branch line integral is simple to evaluate numerically [12]. An increase in complexity arises, however, as complex eigenvalues must be located in order to complete the solution. Further, the fact that each of these complex modes becomes infinite with infinite depth is difficult to understand although the field is computationally correct [10]. Leaky modes which behave improperly for one coordinate are adopted in other fields such as plate vibration [21] and electromagnetic radiation [22] and the series frequently converges rapidly. In addition, the Pekeris branch line integral provides a distinct descriptive device for the lateral wave — a specific physical mechanism.

In the course of this investigation, three distinct types of propagating waves have been isolated. First, there are a finite, sometimes zero, number of trapped modes. These modes are, at long range, traveling cylindrical waves which transmit no energy into the half-space below but, instead, spread cylindrically in the layer. Because the leaky modes and the interface wave decay more rapidly with range, the field in the layer at long range may be adequately represented by the trapped modes alone.

At shorter ranges, the next wave type, the leaky mode, becomes important. These modes are such that their wavefront normals strike the interface with a grazing angle greater than the critical angle. Consequently, energy is transmitted to the half-space. Indeed, the greater the angle, i.e., the higher the mode number, the more energy is transmitted downward through the interface. Except at very short range, a manageable number of these modes is adequate to characterize the leaky field component.

Finally, there is a wave which travels along the interface, continuously radiating energy into both the layer and the half-space. Usually the contribution from this wave is small; however, if a mode is near cutoff, this lateral wave can be excited strongly. Unfortunately, the asymptotic form for this wave field, equation (79), is not valid when a mode is near cutoff and a numerical evaluation of the Pekeris branch line integral must be performed.

Tolstoy [23] has shown that the present model is adequate to predict acoustic propagation in shallow ocean water for both sinusoidal sources and impulsive sources (explosives). While the fluid layer over a fluid half-space is a simplistic model, the concepts developed in this paper can be readily extended to more complicated problems. Addition of fluid layers increases the number of simultaneous equations in the determination of the constants of the depth equations (19). Variation of the sound speed with depth changes the form of these depth equations and requires the use of special functions or numerical integration; however, the solution still reduces to a residue sum plus a branch line integral. Introduction of elastic layers leads to another set of modes and another branch line integral describing the shear wave field. While the solution becomes difficult to implement, the concepts remain unchanged.

Not only is the present technique applicable to the solution of acoustic propagation in fluids and solids: it can be adopted in other field problems. Vibration of submerged plates and electromagnetic wave propagation have already been mentioned. The present problem is also analogous to the problem of nucleus stability in quantum mechanics. In fact, the differential equation, equation (9), is identical in form to the one-dimensional Schroedinger's equation [24]. By analogy, the trapped modes correspond to the discrete bound states of particles "orbiting" the nucleus, and the leaky modes correspond to radioactive states in which particles escape from the nucleus.

ACKNOWLEDGEMENTS

I would like to thank Dr. Richard Llorens of the Pennsylvania State University for his critical review of the manuscript and Mr. Charles Bartberger of NAVAIRDEVCEN for several helpful discussions and suggestions. This work was partially funded under NAVAIR AIRTASK A033370A/001B/1WF11-100-000 and was submitted in partial fulfillment of the requirements for the Master of Engineering degree from Pennsylvania State University.

REFERENCES

1. Lamb, H., "On the propagation of tremors over the surface of an elastic solid," Phil. Trans. Roy. Soc. London, ser. A, 203, pp. 1-42, 1904.

2. Pekeris, C.L., "Theory of propagation of explosive sound in shallow water," Geol. Soc. Am. Memoir 27, 1948.

3. Ewing, W.M., Jardetzky, W.S., and Press, F., ELASTIC WAVES IN LAYERED MEDIA, McGraw-Hill, NY, 1957.

4. Worzel, J.L., and Ewing, W.M., "Explosion sounds in shallow water," Geol. Soc. Am. Memoir 27, 1948.

5. Gutenberg, B., "Dispersion and attenuation of seismic waves," Phys. Zs. 25, pg. 377, 1924.

6. Stoneley, R., "Dispersion of seismic waves," M.N.R.A.S., Geophy. Supp. 1, pg. 280, 1925.

7. Love, A.E.H., SOME PROBLEMS IN GEODYNAMICS, Cambridge University Press, London, 1911.

8. Pekeris, C.L., "Theory of propagation of sound in a half-space of variable sound velocity under conditions of formation of a shadow zone," J. Acoust. Soc. Am. 18, No. 2, pp. 295-315, 1946.

9. Abramowitz, M., and Stegun, I., HANDBOOK OF MATHEMATICAL FUNCTIONS, Dover Publications, NY, 1972.

10. Bartberger, C.L., "Comparison of two normal-mode solutions based on different branch cuts," J. Acoust. Soc. Am. 61, No. 6, pg. 1643, 1977.

11. Stickler, D.C., "Normal-mode program with both the discrete and branch line contributions," J. Acoust. Soc. Am. 57, No. 4, pp. 856-861, 1975.

12. Bucker, H.P., "Propagation in a liquid layer lying over a liquid half-space (Pekeris cut)," J. Acoust. Soc. Am. 65, No. 4, pp. 906-908, 1979.

13. Ingard, U., "On the reflection of a spherical sound wave from an infinite plate," J. Acoust. Soc. Am. 23, No. 3, pp. 329-335, 1951.

14. Clay, C. S., and Medwin, H., ACOUSTICAL OCEANOGRAPHY, John Wiley and Sons, NY, 1977.

15. Stratton, J.A., ELECTROMAGNETIC THEORY, McGraw-Hill, NY, 1941.

16. Brekhovskikh, L.M., WAVES IN LAYERED MEDIA, Academic Press, NY, 1960.

17. Officer, C.B., INTRODUCTION TO THE THEORY OF SOUND TRANSMISSION, McGraw-Hill, NY, 1958.

18. Labianca, F.M., "Normal modes, virtual modes, and alternative representations in the theory of surface duct sound propagation," J. Acoust. Soc. Am. 53, No. 4, pp. 1137-1147, 1973.

19. Williams, A.O., "Pseudoresonances and virtual modes in underwater sound propagation," J. Acoust. Soc. Am. 64, No. 5, pp. 1487-1491, 1978.

20. Tindle, C.T., "Virtual modes and mode amplitudes near cutoff," J. Acoust. Soc. Am. 65, No. 6, pp. 1423-1428, 1979.

21. Stuart, A.D., "Acoustic radiation from submerged plates. I. Influence of leaky wave poles," J. Acoust. Soc. Am. 59, No. 5, pp. 1160-1169, 1976.

22. Marcuvitz, N., "On field representations in terms of leaky modes or eigenmodes," IRE Trans. Ant. and Prop., AP-4, pp. 192-194, 1956.

23. Tolstoy, I., "Shallow water test of the theory of layered wave guides," J. Acoust. Soc. Am. 30, No. 4, pp. 348-361, 1958.

24. Merzbacher, E., QUANTUM MECHANICS, John Wiley and Sons, NY, 1961.

25. Sneddon, I.A., THE USE OF INTEGRAL TRANSFORMS, McGraw-Hill, NY, 1972.

26. Morse, P., and Feshbach, H., METHODS OF THEORETICAL PHYSICS, McGraw-Hill, NY, 1953.

27. Papoulis, A., THE FOURIER INTEGRAL AND ITS APPLICATION, McGraw-Hill, NY, 1962.

28. Churchill, R.V., COMPLEX VARIABLES AND APPLICATIONS, McGraw-Hill, NY, 1960.

APPENDIX A

CYLINDRICAL WAVE EXPANSION OF A SPHERICAL WAVE

APPENDIX A

The expansion of a spherical wave in terms of cylindrical waves can be used to transform a point radiator into a boundary condition. A result of this transformation is that the complications associated with the solution of a non-homogeneous differential equation are avoided.

From the separation of variables solution to the wave equation, the elementary solution, equation (13), to the wave equation in axial symmetry was found to be,

$$\psi = J_o(\gamma r)\, e^{i(\omega t \pm \beta z)} \tag{A-1}$$

where

ψ = velocity potential
γ = horizontal wave number
β = vertical wave number = $\sqrt{k^2 - \gamma^2}$

The superposition integral can be written with the horizontal wave number as a parameter. Thus, after dropping the time dependence of the potential function, we have,

$$\Phi = \int_0^\infty A(\gamma)\, J_o(\gamma r)\, e^{\pm i\beta z}\, d\gamma \tag{A-2}$$

where

A = arbitrary function of γ
Φ = time-independent potential

Recall that a spherical wave can be expressed as the general solution of the wave equation through the following relation,

$$\psi = \frac{f(\omega t - kR)}{R}$$

where

f = arbitrary function describing the waveform
R, radial distance = $\sqrt{r^2 + z^2}$

Following Stratton[15] the wave function corresponding to a harmonic source in cylindrical coordinates may be written as,

$$\psi = \frac{e^{i(\omega t - kR)}}{R} \tag{A-3}$$

After removing the time factor, the wave function in equation (A-3) along the plane z = 0 assumes the form,

$$\Phi(r, o) = \frac{e^{-ikr}}{r} \tag{A-4}$$

Since equation (A-2) represents the general time independent solution to the wave equation, we must determine the function $A(\gamma)$ that reduces the general solution to the spherical wave solution. By substituting $z = 0$ into equation (A-2) and setting the result equal to equation (A-4), we conclude that the equation defining the function $A(\gamma)$ is,

$$\frac{e^{-ikr}}{r} = \int_0^\infty A(\gamma)\, J_0(\gamma r)\, d\gamma \tag{A-5}$$

In order to solve this integral equation, we use the Hankel transform, which is characterized by the following transform pair[25],

$$g(\gamma) = \int_0^\infty f(r)\, J_0(\gamma r)\, r\, dr$$

$$f(r) = \int_0^\infty g(\gamma)\, J_0(\gamma r)\, \gamma\, d\gamma \tag{A-6}$$

Replacing $A(\gamma)$ by $\gamma g(\gamma)$ in equation (A-5), we have,

$$\frac{e^{-ikr}}{r} = f(r) = \int_0^\infty g(\gamma)\, J_0(\gamma r)\, \gamma\, d\gamma \tag{A-7}$$

Using the first of equations (A-6), we can reduce this last equation to,

$$g(\gamma) = \int_0^\infty e^{-ikr}\, J_0(\gamma r)\, dr$$

Moreover, the Bessel function J_0 can be replaced by its integral expansion to yield[9],

$$g(\gamma) = \frac{1}{2\pi} \int_{-\pi}^{\pi} \int_0^\infty e^{-ir(k-\gamma \cos\theta)}\, dr d\theta \tag{A-8}$$

The integration over r is elementary provided that k possesses a negative imaginary part. If we make this imaginary part arbitrarily small, we obtain,

$$g(\gamma) = \frac{1}{2\pi i} \int_{-\pi}^{\pi} \frac{d\theta}{k - \gamma \cos\theta} \tag{A-9}$$

By introducing the transformation $u = e^{i\theta}$ into equation (A-9), the integral may be expressed as a contour integration in the complex plane,

$$g(\gamma) = \frac{1}{\pi\gamma} \int_C \frac{du}{u^2 - 2uk/\gamma + 1}$$

where C, the contour = the unit circle.

To evaluate the integral using the residue theorem, we must first determine the roots of the denominator which are given by,

$$\begin{aligned} u^2 - 2uk/\gamma + 1 &= (u - u_1)(u - u_2) \\ &= u^2 + u(u_1 + u_2) + u_1 u_2 \end{aligned} \tag{A-10}$$

Comparing the constant terms of this last result, we find,

$$u_1 u_2 = 1$$

It is apparent from this result that one root must lie inside the unit circle and the other must lie outside. Since only the root inside the unit circle contributes to the contour integral, we must examine the magnitude of the roots. Therefore, solving the quadratic equation, (A-10) for u,

$$u = \frac{k \pm \sqrt{k^2 - \gamma^2}}{\gamma}$$

Further, the residue at the smaller root is equal to,

$$\text{res} = \frac{1}{(u_1 - u_2)} = \frac{-\gamma}{2\sqrt{k^2 - \gamma^2}}$$

Finally, the integral in equation (A-9) can be written as,

$$g(\gamma) = \frac{-i}{\sqrt{k^2 - \gamma^2}} \tag{A-11}$$

Introducing this last result into equation (A-7), we find that on the plane z = 0,

$$\frac{e^{-ikr}}{r} = \int_0^\infty \frac{\gamma J_0(\gamma r)}{i\sqrt{k^2 - \gamma^2}}\, d\gamma$$

Combining equations (A-2), (A-5), and this last result, we find that the velocity potential of a spherical wave is,

$$\psi = e^{i\omega t} \int_0^\infty \frac{J_0(\gamma r)\, e^{\pm i\beta z}}{i\beta}\, \gamma d\gamma \tag{A-12}$$

APPENDIX B

PROOF OF THE VALIDITY OF THE RESIDUE SUM/BRANCH LINE INTEGRAL SOLUTION

APPENDIX B

In the process of deriving the solution to the field equation, equation (24), in terms of a sum of residues and a branch line integral, equation (45), we assumed that the integrals over contours C_1, C_2, C_3 and C_4, shown in figure 2, vanish as the radius of these arcs becomes infinite. Indeed, we shall show that this conclusion is valid provided the source-to-observation-point range is not zero; that is, provided the observation point is neither directly above nor directly below the source.

Employing equation (31), we can write the required integrals in the following form,

$$\int_{C_{1234}} = \int_{C_{1234}} H_o^{(2)}(\gamma r)\, \gamma\, G(\beta_1, \beta_2)\, d\gamma \tag{B-1}$$

where C_{1234} = any of the contours, C_1, C_2, C_3, C_4 shown in figure 2.

For very large values of the horizontal wave number γ, equations (18) reduce, approximately to,

$$\beta_{1,2}^2 \sim -\gamma^2$$

or,

$$\beta_{1,2} \sim \pm i\gamma$$

Observe that the sign of the above expression depends on the location of the contour with respect to the branch cuts shown in figure 2.

From the correspondence between the β and γ-planes illustrated in figure 3, we notice that:

a) along C_1 and C_2,

$$\beta_{1,2} = i\gamma \tag{B-2}$$

b) along C_3,

$$\beta_1 = i\gamma$$
$$\beta_2 = -i\gamma \tag{B-3}$$

c) along C_4,

$$\beta_{1,2} = -i\gamma \tag{B-4}$$

Also, along these circular arc contours, γ is given by,

$$\gamma = Re^{i\phi} \tag{B-5}$$

where

$R \to \infty$

ϕ = angular position along contour.

As a consequence of this last result, the differential element, $d\gamma$, can be written as,

$$d\gamma = iRe^{i\phi}\, d\phi \tag{B-6}$$

Further, the Hankel function in the integrand of equation (B-1) can be expressed in terms of the asymptotic approximation, equation (29). Using equation (B-5) for the wave number, we can then write,

$$\gamma H_o^{(2)}(\gamma r) \simeq \sqrt{\frac{2}{\pi r}}\, (Re^{i\phi})^{1/2}\, e^{i\frac{\pi}{4}}\, e^{-irRe^{i\phi}} \tag{B-7}$$

In order to proceed with the analysis, we must consider each contour separately. Along the contour C_1, the angle ϕ ranges from $-\pi$ to $-\pi/2$ and the vertical wave numbers, β_1 and β_2, are given by equation (B-2). Substituting these values for β_1 and β_2 into the equation defining $G(\beta_1, \beta_2)$, equation (30), and replacing γ with the right side of equation (B-5), we can show that,

$$G(\beta_1, \beta_2) = -\frac{1}{2}(Re^{i\phi})^{-1}\, e^{-R(z-d)\cos\phi}\, e^{iR(z-d)\sin\phi}$$

Observe that terms that decrease exponentially as R increases to infinity have been deleted from this last equation. After this last result is combined with equations (B-7) and (B-6), the contour integral given by equation (B-1) may be written,

$$\int_{C_1} = -ie^{i\frac{\pi}{2}} \sqrt{\frac{R}{2\pi r}} \int_{-\pi}^{-\pi/2} \left\{ (e^{i\phi})^{1/2}\, e^{R[r\sin\phi + (z-d)\cos\phi]} \cdot e^{-iR[r\cos\phi - (z-d)\sin\phi]} \right\} d\phi$$

Consequently,

$$\left| \int_{C_1} \right| \leq \sqrt{\frac{R}{2\pi r}} \int_{-\pi}^{-\pi/2} e^{R[r\sin\phi + (z-d)\cos\phi]}\, d\phi \tag{B-8}$$

Over the range of ϕ given by the limits of integration, the following inequalities are valid,

$$e^{-2rR\left(\frac{\phi}{\pi} + 1\right)} \geqslant e^{rR\sin\phi}$$

$$e^{2R(z-d)\left(\frac{\phi}{\pi} + 1\right)} \geqslant e^{R(z-d)\cos\phi}$$

Hence, equation (B-8) can be reduced to the following form,

$$\left| \int_{C_1} \right| \leqslant \sqrt{\frac{R}{2\pi r}}\, e^{R(z-d-2r)} \int_{-\pi}^{-\pi/2} e^{\frac{2R\phi}{\pi}(z-d-r)}\, d\phi$$

Or,

$$\left| \int_{C_1} \right| \leq \sqrt{\frac{\pi}{8R}} \left[\frac{e^{-rR} - e^{-R(z-d)}}{(z-d-r)} \right] \tag{B-9}$$

Observe that the right side of equation (B-9) vanishes as R becomes infinite. Thus, the integral along the contour C_1 can be neglected unconditionally.

Since $G(\beta_1, \beta_2)$ is an even function of β_2 (A consequence of equation (30)) and the sign of β_1 remains positive along C_2 and C_3 (see equations (B-2) and (B-3)), equation (B-8) can be applied along these contours to prove that,

$$\left| \int_{C_{2,3}} \right| \leq \sqrt{\frac{R}{2\pi r}} \int_{-\pi/2}^{\phi_o} e^{R[r \sin \phi + (z-d) \cos \phi]} \, d\phi \tag{B-10}$$

Introducing a change of variables, we write,

$$x = R \cos \phi$$
$$x_o = R \cos \phi_o$$
$$dx = -R \sin \phi \, d\phi$$

where

x = distance along the real γ axis
x_o = distance from origin to either γ_2 (for C_2) or γ_1 (for C_3)
ϕ_o = upper limit of ϕ for appropriate contour.

Thus, equation (B-10) becomes,

$$\left| \int_{C_{2,3}} \right| \leq \sqrt{\frac{R}{2\pi f}} \int_{o}^{x_o} e^{rR \sin \phi} e^{x(z-d)} \frac{dx}{R \sin \phi} \tag{B-11}$$

In addition, the following inequalities are valid over the range of x indicated by the limits of integration,

$$\frac{dx}{R \sin \phi_o} > \frac{dx}{R \sin \phi}$$

$$e^{rR \sin \phi_o} > e^{rR \sin \phi}$$

Hence, equation (B-11) can be reduced to the folloiwng form,

$$\left| \int_{C_{2,3}} \right| \leq \frac{e^{rR \sin \phi_o}}{\sqrt{2\pi r R \sin \phi_o}} \int_{o}^{x_o} e^{x(z-d)} \, dx$$

Integrating the above and observing that, as R becomes infinite ϕ_o approaches $-\pi/2$, we write,

$$\left| \int_{C_{2,3}} \right| \leq \frac{e^{-rR}}{(z-d)\sqrt{2\pi rR}} \left[e^{x_o(z-d)} - 1 \right] \tag{B-12}$$

We can show from this last result that the integrals over contours C_2 and C_3 vanish provided the radius r is not zero.

According to equation (B-4), the sign of β_1 is negative along C_4; therefore, the expression for $G(\beta_1, \beta_2)$, i.e., equation (30), has the following form,

$$G(\beta_1, \beta_2) = -\frac{1}{2}(Re^{i\phi})^{-1} e^{-R(z-d)\cos\phi} e^{-iR(z-d)\sin\phi}$$

Substituting this last result and equations (B-6) and (B-7) into equation (B-1), we can write the contour integral along C_4 as,

$$\left| \int_{C_4} \right| = -ie^{i\frac{\pi}{4}} \sqrt{\frac{R}{2\pi r}} \int_{-\pi/2}^{o} (e^{i\phi})^{1/2} e^{R[r\sin\phi - (z-d)\cos\phi]}$$

$$\cdot e^{-iR[r\cos\phi + (z-d)\sin\phi]} \, d\phi$$

Therefore,

$$\left| \int_{C_4} \right| \leq \sqrt{\frac{R}{2\pi r}} \int_{-\pi/2}^{o} e^{R[r\sin\phi - (z-d)\cos\phi]} \, d\phi \tag{B-13}$$

Within the range of ϕ given by the above limits of integration, the following inequalities are valid,

$$e^{\frac{2rR\phi}{\pi}} \geq e^{rR\sin\phi}$$

$$e^{-R(z-d)\frac{2}{\pi}(\phi + \frac{\pi}{2})} \geq e^{-R(z-d)\cos\phi}$$

Hence, equation (B-13) reduces to the form,

$$\left| \int_{C_4} \right| \leq \sqrt{\frac{R}{2\pi r}} e^{-R(z-d)} \int_{-\pi/2}^{o} e^{\frac{2R\phi}{\pi}(r-z+d)} \, d\phi$$

Integrating, we see that,

$$\left| \int_{C_4} \right| \leq \sqrt{\frac{\pi}{8rR}} \left[\frac{e^{-R(z-d)} - e^{-rR}}{r-z+d} \right]$$

This last result vanishes unconditionally as R increases to infinity. Thus, we have shown that all of the circular arc contours, C_1, C_2, C_3 and C_4, in figure 2 contribute nothing to the field provided that the radius, r, is not zero.

APPENDIX C

LOCATION OF THE EIGENVALUES

APPENDIX C

The eigenvalues corresponding to the normal modes of the layered half-space are the values of γ which satisfy equation (33),

$$\beta_1 \cos \beta_1 H + ib\beta_2 \sin \beta_1 H = 0 \tag{C-1}$$

where

$$\beta_{1,2} = \sqrt{\frac{\omega^2}{c_{1,2}^2} - \gamma^2}$$

Solutions to equation (C-1) are possible, for real γ, if

$$\frac{\omega}{c_2} < \gamma < \frac{\omega}{c_1}$$

Introducing these values of γ into equation (C-1), we discover that β_1 is real and β_2 is imaginary. Under these conditions, the characteristic equation (C-1) becomes,

$$\frac{\sqrt{\frac{\omega^2}{c_1^2} - \gamma_n^2}}{\sqrt{\gamma_n^2 - \frac{\omega^2}{c_2^2}}} = -b \tan \sqrt{\frac{\omega^2}{c_1^2} - \gamma_n^2}\ H \tag{C-2}$$

These modes are trapped modes with phase velocities between c_1 and c_2 and real eigenvalues, γ_n.

In order to locate the complex roots of equation (C-1), we will transform the variables as follows[3],

$$\nu_{1,2}^2 = -\beta_{1,2}^2 = \gamma^2 - \frac{\omega^2}{c_{1,2}^2} \tag{C-3}$$

Selecting the sign of the square root by the same argument used in deriving equation (21), we can write,

$$-i\nu_{1,2} = \beta_{1,2} \tag{C-4}$$

Substituting this last result into equation (C-1), we find that,

$$\nu_1 + b\,\nu_2 \tanh \nu_1 H = 0 \tag{C-5}$$

If ν is complex, equation (C-5) can be separated into real and imaginary parts,

$$\nu_{1r} - \nu_{1i} \tanh \nu_{1r} H \tan \nu_{1i} H + b\nu_{2r} \tanh \nu_{1r} H - b\nu_{2i} \tan \nu_{1i} H = 0$$

$$\nu_{1i} + \nu_{1r} \tanh \nu_{1r} H \tan \nu_{1i} H + b\nu_{2r} \tan \nu_{1i} H + b\nu_{2i} \tanh \nu_{1r} H = 0$$

where

ν_{1r} = real part of ν_1

ν_{1i} = imaginary part of ν_1

ν_{2r} = real part of ν_2

ν_{2i} = imaginary part of ν_2

Eliminating tan $\nu_{1i}H$ from the above two equations, so that we may eliminate the periodic change in sign, we may write,

$$\frac{\nu_{1r} + b\,\nu_{2r} \tanh \nu_{1r} H}{\nu_{1i} + b\,\nu_{2i} \tanh \nu_{1r} H} = - \left[\frac{b\,\nu_{2i} + \nu_{1i} \tanh \nu_{1r} H}{b\,\nu_{2r} + \nu_{1r} \tanh \nu_{1r} H} \right] \tag{C-6}$$

In each region of the γ-plane shown in figure 3, the signs of the components of ν_1 and ν_2 possess definite values. Using this figure and equation (C-1), the signs can be determined and introduced into equation (C-6). As a consequence, we find that complex eigenvalues can not exist in any region of the γ-plane except region I. All the other combinations of sign lead to a positive quantity on one side of equation (C-6) and a negative quantity on the other.

In view of this analysis, we see that the complex eigenvalues are located in the fourth quadrant of the γ plane to the left of the branch cut from ω/c_2. Therefore, the EJP cut possesses no complex eigenvalues since region I does not exist for this cut.

To show that an infinite number of complex eigenvalues exist for the Pekeris cut, consider the location of eigenvalues for large γ. In this case, equation (C-3) can be written,

$$\nu_{1,2} \simeq \gamma$$

Substituting this last result into equation (C-5), we discover that,

$$-\frac{1}{b} = \tanh \gamma_1 H = \frac{\sinh 2\gamma_r H + i \sin 2\gamma_i H}{\cosh 2\gamma_r H + \cos 2\gamma_i H} \tag{C-7}$$

where

γ_r = real part of γ

γ_i = imaginary part of γ

Since b is real,

$$\sin 2\gamma_i H = 0$$

This last result is equivalent to the statement,

$$\gamma_i = \frac{n\pi}{2H} \tag{C-8}$$

where n = large integer.

Introducing this last equation into equation (C-7), we can write,

$$-\frac{\rho_2}{\rho_1} = \frac{\sinh 2\gamma_r H}{\cosh 2\gamma_r H \pm 1}$$

By solving the above equation for γ_r, we discover that the real part of these eigenvalues asymptotically approaches the value,

$$\gamma_r = \frac{1}{2H} \ell n \left| \frac{b+1}{b-1} \right| \qquad \text{(C-9)}$$

Thus, equations (C-9) and (C-8) describe the positions of these complex eigenvalues for large γ. In particular, equation (C-8) demonstrates that there are an infinite number of these eigenvalues.

APPENDIX D

PLANE WAVE EXPANSION OF A SPHERICAL WAVE

APPENDIX D

Since the behavior of plane waves at an interface between two media is well known[14], we will examine the expansion of a spherical wave in terms of plane waves. The derivation given below follows Brekhovskikh[16]; however, in order to facilitate comparisons with material in this paper, the results are presented in wave number space rather than in terms of the complex angle of incidence.

The elementary harmonic plane wave function is given by,

$$\psi = e^{i(\omega t - K \cdot \mathcal{R})} \tag{D-1}$$

where

K, vector wave number = $\gamma_x i + \gamma_y j + \beta k$

$\mathcal{R}$, range vector = $xi + yj + zk$

x, y, z = observation point coordinates

$\gamma_x, \gamma_y, \beta$ = plane wave number coordinates

In accordance with the work of Appendix A, the spherical wave can be written as a superposition of these elementary functions along z = 0, thus,

$$\frac{e^{-ikr}}{r} = \int_{-\infty}^{\infty}\int A(\gamma_x, \gamma_y)\, e^{\,i(\gamma_x x + \gamma_y y)}\, d\gamma_x d\gamma_y \tag{D-2}$$

This last result is a two-dimensional Fourier transform; therefore, the inverse transform will yield[25],

$$A(\gamma_x, \gamma_y) = \frac{1}{4\pi^2} \int_{-\infty}^{\infty}\int \frac{e^{-ikr}}{r}\, e^{\,i(\gamma_x x + \gamma_y y)}\, dxdy \tag{D-3}$$

This integral can be converted to polar coordinates by employing the following transformation,

$$\begin{aligned} x &= r\cos\theta \\ y &= r\sin\theta \\ \gamma_x &= \gamma\cos\phi \\ \gamma_y &= \gamma\sin\phi \end{aligned} \tag{D-4}$$

where

γ = horizontal wave number

ϕ = angular coordinate of γ shown in figure 5.

Furthermore, the element of area in the transformed space is $\gamma d\gamma d\theta$. Substitution of equations (D-4) in equation (D-3) changes the integral form to,

$$A(\gamma_X, \gamma_Y) = \frac{1}{4\pi^2} \int_0^{\infty} \int_0^{2\pi} e^{-i\gamma r[k - \gamma \cos(\theta - \phi)]} \, d\theta d\gamma$$

This last integral is identical in form with equation (A-8) so that the evaluation procedure discussed in Appendix A may be applied. Thus, we find,

$$A(\gamma_X, \gamma_Y) = \frac{-i}{2\pi\sqrt{k^2 - \gamma^2}} \tag{D-5}$$

Substituting this value of A into equation (D-2), we have,

$$\frac{e^{-ikr}}{r} = \frac{-i}{2\pi} \int\int_{-\infty}^{\infty} \frac{e^{-i(\gamma_X x + \gamma_Y y)}}{\sqrt{k^2 - \gamma^2}} \, d\gamma_X \, d\gamma_Y$$

Writing this last result in terms of the wave number vector and extending the investigation to include the z direction, we may represent the velocity potential as,

$$\psi = \frac{e^{i\omega t}}{2\pi} \int\int_{-\infty}^{\infty} \frac{e^{-i\vec{K} \cdot \vec{R}}}{i\beta} \, d\gamma_X \, d\gamma_Y \tag{D-6}$$

where β, vertical wave number $= \sqrt{k^2 - \gamma^2}$ as illustrated in figure 5.

This last expression is the expansion of a spherical wave in terms of plane waves.

Observe from the geometry of figure 5 and the fact that k is a constant, that, as γ_X and γ_Y assume progressively larger values, β becomes imaginary. Waves having imaginary wave numbers are called inhomogeneous waves. When we consider the exponential part of these waves (from equation (D-1)), their nature becomes evident.

$$e^{i(\omega t - \gamma_X X - \gamma_Y Y + \beta z)} = e^{i(\omega t - \gamma_X X - \gamma_Y Y)} \, e^{-\alpha z} \qquad (z > 0)$$

where

α = positive real number

$\beta = i\alpha$.

Hence, this wave propagates horizontally and is damped in an exponential manner in both directions vertically away from the plane, z = 0.

Finally, equation (D-6) is equivalent to the expansion of a spherical wave in terms of cylindrical waves as given by equation (A-12). This correspondence can be demonstrated by applying the transformation defined by equations (D-4) to equation (D-6). As γ_X and γ_Y are altered from $-\infty$ to ∞, γ assumes values from zero to infinity and ϕ varies from zero to 2π. In addition, the

differential element equivalent to $d\gamma_x d\gamma_y$ is $\gamma d\gamma d\phi$. If we apply this transformation to equation (D-6), we can write,

$$\psi = \frac{-ie^{i\omega t}}{2\pi} \int_0^{\infty} \int_0^{2\pi} \frac{e^{-i\gamma r(\sin\phi \sin\theta + \cos\phi \cos\theta)} e^{\pm i\beta z}}{\beta} \gamma d\gamma d\phi$$

$$= -ie^{i\omega t} \int_0^{\infty} \frac{\gamma e^{\pm i\beta z}}{\beta} \left[\frac{1}{2\pi} \int_0^{2\pi} e^{-i\gamma r \cos(\phi - \theta)} d\phi \right] d\gamma$$

The quantity in the brackets of the above integral is equivalent to an integral form of the Bessel function[9], $J_o(\gamma r)$, therefore,

$$\psi = e^{i\omega t} \int_0^{\infty} \frac{J_o(\gamma r) e^{\pm i\beta z}}{i\beta} \gamma d\gamma \qquad \text{(D-7)}$$

This last result is identical with equation (A-12).

APPENDIX E

BOUNDARY VALUE PROBLEM FOR TWO FLUID HALF-SPACES

APPENDIX E

Determination of the field induced in a fluid by a point source above a fluid half-space requires a procedure analogous to the technique employed in the body of this paper. Figure 4 illustrates the physical problem in which the lower half-space is a homogeneous fluid of sound speed, c_2, and density, ρ_2. Depth functions corresponding to equations (19) can be written.

$$\begin{aligned} Z_1 &= C_1 e^{-i\beta_1 z} && (d < z < \infty) \\ Z_2 &= C_2 e^{-i\beta_1 z} + C_3 e^{i\beta_1 z} && (0 < z < d) \\ Z_3 &= C_4 e^{i\beta_2 z} && (z < 0) \end{aligned} \tag{E-1}$$

Boundary conditions applicable to this problem are: (a) continuity of pressure at z = 0; (b) continuity of particle velocity at z = 0; (c) continuity of pressure at the source depth; and (d) a discontinuity of particle velocity at the source depth representing the point source. In mathematical terms, these conditions are,

$$\begin{aligned} &\text{(a)} \quad \rho_1 Z_2 = \rho_1 Z_3 && \text{at } z = 0 \\ &\text{(b)} \quad \frac{dZ_2}{dz} = \frac{dZ_3}{dz} && \text{at } z = 0 \\ &\text{(c)} \quad Z_1 = Z_2 && \text{at } z = d \\ &\text{(d)} \quad \frac{dZ_2}{dz} - \frac{dZ_1}{dz} = 2\gamma && \text{at } z = d \end{aligned} \tag{E-2}$$

From these conditions, we can determine the constants in equations (E-1) and write the depth function in the region below the source and above the interface,

$$Z_2 = \frac{\gamma}{i\beta_1} \left\{ e^{-i\beta_1 (z+d)} \left[\frac{\beta_1 - b\beta_2}{\beta_1 + b\beta_2} \right] + e^{-i\beta_1 (d-z)} \right\} \quad (0 < z < d) \tag{E-3}$$

where b, density ratio = ρ_1/ρ_2

Finally, by employing a superposition similar to that of equation (15), the solution for the velocity potential is,

$$\begin{aligned} \psi_2 = e^{i\omega t} \int_0^\infty J_0(\gamma r) \frac{e^{-i\beta_1 (d-z)}}{i\beta_1} \gamma d\gamma \\ + e^{i\omega t} \int_0^\infty J_0(\gamma r) \frac{e^{-i\beta_1 (d+z)}}{i\beta_1} \left[\frac{\beta_1 - b\beta_2}{\beta_1 + b\beta_2} \right] \gamma d\gamma \end{aligned} \tag{E-4}$$

APPENDIX F

METHOD OF STEEPEST DESCENT

APPENDIX F

The method of steepest descent, or saddle point method, is a technique for approximating complex contour integrals. If the integrand satisfies certain conditions, a region in the complex plane can be located that contributes most of the integral's value. By considering the poles and branches of the function, the original contour can be deformed so that it passes through this region. Furthermore, the path is selected so that the function decreases as quickly as possible on each side of this region. By requiring that a parameter in the integrand be large, the descent in either direction becomes steep and only the behavior of the function near a single point need be considered.

Hence, the problem is one of locating the saddle point where the peak value of the integrand occurs, finding the path of steepest descent away from the saddle point, deforming the original contour into the descent path and writing a series approximation for the integral.[3,16,26,27] This appendix follows the method of Brekhovskikh[16] although a more direct technique for obtaining the asymptotic series is introduced.

The method of steepest descent may be applied to integrals of the form,

$$I = \int_c G(\alpha)\, e^{\rho f(\alpha)}\, d\alpha \qquad \text{(F-1)}$$

where

- c = contour in the α-plane
- G, f = analytic functions
- I = complex integral
- α = independent complex variable
- ρ = positive real number

We consider the evaluation of this integral for large values of ρ.

Generally, f is a complex function which can be written as the sum of a real and an imaginary part,

$$f(\alpha) = f_1(\alpha) + i f_2(\alpha)$$

Furthermore,

$$e^{\rho f} = e^{\rho f_1}\, e^{i\rho f_2} \qquad \text{(F-2)}$$

Thus, f_1 controls the magnitude of the exponential while f_2 defines its phase. We must find a point, α_o, at which the function f_1 is maximum and determine a contour for which f_1 decreases most rapidly on either side of α_o.

In order to locate α_o and the path of descent, we must consider the properties of $f(\alpha)$ as an analytic function of the complex variable α. Since the function is analytic, the Cauchy-Riemann conditions[28] apply,

$$\frac{\partial f_1}{\partial x} = \frac{\partial f_2}{\partial y}$$

$$\frac{\partial f_1}{\partial y} = -\frac{\partial f_2}{\partial x} \qquad \text{(F-3)}$$

A stationary point of f_1 is obtained if,

$$\frac{\partial f_1}{\partial x} = \frac{\partial f_1}{\partial y} = 0$$

Equations (F-3) imply that the above conditions are also valid for the function f_2. If we assume that f_1 is a maximum with respect to x, then,

$$\frac{\partial^2 f_1}{\partial x^2} = \frac{\partial^2 f_2}{\partial x \partial y} < 0$$

Differentiating the second of equations (F-3) with respect to y, we find,

$$\frac{\partial^2 f_1}{\partial y^2} = -\frac{\partial^2 f_1}{\partial x \partial y} > 0$$

This last result demonstrates that if f_1 is a maximum with respect to x, then, it is a minimum with respect to y.

Hence, we conclude that for analytic functions a stationary point will not correspond to an absolute maximum or minimum of the function. If the function f_1 (x, y) possesses a maximum in one direction, we obtain a minimum at 90° to this direction. For this reason, a stationary point of an analytic function is called a saddle point after the saddle surface to which it corresponds. From the saddle, we find peaks in two opposite directions and valleys in the other two perpendicular directions. The desired path of integration passes from the saddle point through these valleys, one on each side of the saddle. This path concentrates the significant part of the integration in the shortest possible interval.

We recall that the direction of most rapid change of a function is given by the gradient of the function,

$$\nabla f_1 = \frac{\partial f_1}{\partial x}\, i + \frac{\partial f_1}{\partial y}\, j$$

Further, the slope of this vector in the x, y-plane is given by,

$$\frac{dy}{dx} = \frac{\partial f_1/\partial y}{\partial f_1/\partial x}$$

According to equation (F-3), we may write this last result as,

$$\frac{dy}{dx} = -\frac{\partial f_2/\partial x}{\partial f_2/\partial y} \qquad \text{(F-4)}$$

For the path of constant f_2, we have,

$$df_2 = \frac{\partial f_2}{\partial x}\, dx + \frac{\partial f_2}{\partial y}\, dy = 0$$

This last relation is identical to equation (F-4). In other words, the direction of most rapid change of f_1 corresponds to the direction of constant f_2. Since f_2 determines the phase of the exponential in equation (F-2), the path of steepest descent coincides with the path of constant phase.

Thus, the saddle point is determined by the condition,

$$\left.\frac{df}{d\alpha}\right|_{\alpha_o} = 0 \qquad \text{(F-5)}$$

Furthermore, the required descent path must be a path over which the imaginary part of f remains constant and the real part decreases on both sides of the saddle point. By introducing an, as yet, undetermined parameter, we can describe the behavior of f along the descent path as follows,

$$f(\alpha) = f(\alpha_o) - s^2 \qquad (-\infty < s < \infty) \qquad \text{(F-6)}$$

where s = real-valued parameter.

If we can determine the path in the α-plane along which equation (F-6) is true, we have located the path of steepest descent.

By employing equation (F-6), we can write equation (F-1) in the following form,

$$I = e^{\rho f(\alpha_o)} \int_C G(\alpha)\, e^{-\rho s^2}\, d\alpha \qquad \text{(F-7)}$$

We shall alter the variable of integration to s by introducing a function $\xi(s)$ which is defined by,

$$\xi(s)ds = G(\alpha)d\alpha \qquad \text{(F-8)}$$

Introducing equation (F-8) into equation (F-7), we have,

$$I = e^{\rho f(\alpha_o)} \int_{-\infty}^{\infty} \xi(s)\, e^{-\rho s^2}\, ds \qquad \text{(F-9)}$$

Since ρ is large, only small values of s contribute significantly to the integral. Therefore, we can expand ξ in powers of s and retain only the first few terms of such an expansion. In this manner, equation (F-9) becomes,

$$I \simeq e^{\rho f(\alpha_o)} \left\{ \xi(o) \int_{-\infty}^{\infty} e^{-\rho s^2}\, ds + \frac{1}{2}\, \xi''(o) \int_{-\infty}^{\infty} s^2\, e^{-\rho s^2}\, ds \right\}$$

Note that terms with odd powers of s when integrated yield zero since the integration is between limits symmetric around zero. The resulting integrals have been tabulated in the literature so that the approximation to the original integral, equation (F-1), is,

$$I = e^{\rho f(\alpha_o)} \sqrt{\frac{\pi}{\rho}} \left\{ \xi(o) + \frac{1}{4\rho} \xi''(o) \right\} \tag{F-10}$$

To complete the analysis, we must find an expression for ξ in terms of known functions. From equation (F-6), we may write,

$$\frac{df}{d\alpha} = f' = -2s \frac{ds}{d\alpha}$$

Combining this last result with equation (F-8), we find,

$$\xi(s) = \frac{-2sG}{f'} \tag{F-11}$$

Each of the functions on the right side of equation (F-11) can be expanded in a Taylor series, thus,

$$G(x) = G(o) + x\,G'(o) + \frac{x^2}{2} G''(o) + \ldots$$

thus, (F-12)

$$f'(x) = xf''(o) + \frac{x^2}{2} f'''(o) + \frac{x^3}{3!} f''''(o) + \ldots$$

where $x = \alpha - \alpha_o$.

From equation (F-6), we conclude that,

$$s^2 = -\frac{x^2}{2} f''(o) - \frac{x^3}{3!} f'''(o) - \frac{x^4}{4!} f''''(o) - \ldots$$

Introducing this last expression and equations (F-12) into equation (F-11), we have,

$$\xi(s) = \frac{-2\sqrt{-\frac{1}{2}f'' - \frac{x}{6}f''' - \frac{x^2}{24}f''''}}{f'' + \frac{x}{2}f''' + \frac{x^2}{6}f''''} \left[G + x\,G' + \frac{x^2}{2} G'' \right] \tag{F-13}$$

Hence, the first term of equation (F-10) is given by,

$$\xi(o) = -\sqrt{\frac{-2}{f''(\alpha_o)}}\; G(\alpha_o) \tag{F-14}$$

Note that in this last evaluation, when $x = s = 0$, then, $\alpha = \alpha_o$. Differentiating equation (F-13) twice with respect to s, we obtain the second term of equation (F-10), i.e.,

$$\xi''(o) = 2\xi(o) \left[\frac{f'''G'}{(f'')^2 G} - \frac{5(f''')^2}{12(f'')^3} + \frac{f''''}{4(f'')^2} - \frac{G''}{f''G} \right] \tag{F-15}$$

Observe that all the quantities in equation (F-15) must be evaluated at $\alpha = \alpha_o$.